

# The sensitivity of stellar feedback to IMF averaging versus IMF sampling in galaxy formation simulations

Matthew C. Smith<sup>1,2</sup>★

<sup>1</sup> *Harvard-Smithsonian Center for Astrophysics, 60 Garden Street, Cambridge, MA 02138, USA*

<sup>2</sup> *Center for Computational Astrophysics, Flatiron Institute, 162 5<sup>th</sup> Avenue, New York, NY 10010, USA*

6 June 2022

## ABSTRACT

Galaxy formation simulations frequently use Initial Mass Function (IMF) averaged feedback prescriptions, where star particles are assumed to represent single stellar populations that fully sample the IMF. This approximation breaks down at high mass resolution, where stochastic variations in stellar populations become important. We discuss various schemes to populate star particles with stellar masses explicitly sampled from the IMF. We use Monte Carlo numerical experiments to examine the ability of the schemes to reproduce an input IMF in an unbiased manner while conserving mass. We present our preferred scheme which can easily be added to pre-existing star formation prescriptions. We then carry out a series of high resolution isolated simulations of dwarf galaxies with supernovae, photoionization and photoelectric heating to compare the differences between using IMF averaged feedback and explicitly sampling the IMF. We find that if supernovae are the only form of feedback, triggering individual supernovae from IMF averaged rates gives identical results to IMF sampling. However, we find that photoionization is more effective at regulating star formation when IMF averaged rates are used, creating more, smaller H II regions than the rare, bright sources produced by IMF sampling. We note that the increased efficiency of the IMF averaged feedback versus IMF sampling is not necessarily a general trend and may be reversed depending on feedback channel, resolution and other details. However, IMF sampling is always the more physically motivated approach. We conservatively suggest that it should be used for star particles less massive than  $\sim 500 M_{\odot}$ .

**Key words:** galaxies: formation, galaxies: evolution, methods: numerical

## 1 INTRODUCTION

Substantial progress in understanding the formation and evolution of galaxies has been made over the last few decades by accounting for the role played by stellar feedback (see e.g. the reviews of Somerville & Davé 2015; Naab & Ostriker 2017, and the references therein). Stars interact with the gas inside galaxies and beyond via a variety of complex processes, including supernovae (SNe), stellar winds and radiation (providing photoionization, photodissociation, photoheating and radiation pressure). They can therefore act to influence the thermal and kinetic state of the interstellar medium (ISM), regulate star formation, enrich gas with metals, drive galactic outflows (carrying metals out into the circumgalactic medium (CGM)) and more besides. As the preferred terminology, “feedback”, would suggest, these processes represent a back-reaction on the gas from which stars

themselves originate. Thus, numerical simulations of galaxies must account for the gaseous and stellar components, as well as their interactions, in a self-consistent manner.

The “star particle” has been a nearly ubiquitous feature of hydrodynamic simulations of galaxy formation for nearly three decades (see early examples in e.g. Katz 1992; Katz et al. 1996; Navarro & White 1993; Mihos & Hernquist 1994). In the majority of cases, the star particle does not represent individual stars or even star clusters, per se. It instead traces an underlying collisionless stellar fluid in much the same way that a dark matter particle traces the dark matter fluid. Unlike the dark matter component, however, the stellar component must interact with the gas through processes in addition to gravity. Star particles can be created from gas mass to represent the process of star formation. Stellar feedback can be directly tied to the star particle (as in Katz 1992, one of the first examples of stellar feedback being explicitly included in a simulation). However, when the mass resolution is low, some or all of the stellar feed-

★ E-mail: matthew.smith@cfa.harvard.edu

back may not be directly associated with star particles but instead associated with the star forming gas. For example, [Springel & Hernquist \(2003\)](#) presents models which treat unresolved SN feedback by modifying the equation of state of star forming gas and launching stellar feedback driven winds from the gas without directly involving a star particle. There is no inconsistency in this context as the star particle does not explicitly represent the location of the stellar mass, which is in some sense smoothed over the ensemble of particles. Such “diffuse” stellar feedback models are frequently used in modern large volume cosmological simulations, usually in combination with star particle centred feedback to a greater or lesser extent ([Vogelsberger et al. 2013, 2014](#); [Dubois et al. 2014, 2016](#); [Davé et al. 2016, 2019](#); [Pillepich et al. 2018](#)). Once the mass resolution of the star particle approaches  $\sim 10^4 M_\odot$  or better, stellar feedback is usually tied directly to star particles and is modelled in a more explicit manner (for a small sample of contemporary approaches see e.g. [Hopkins et al. 2014](#); [Hopkins et al. 2018](#); [Ceverino et al. 2014](#); [Kimm et al. 2015](#); [Agertz & Kravtsov 2015](#); [Marinacci et al. 2019](#)). This is appropriate because the lower particle masses begin to allow small scale spatial and temporal clustering of feedback processes to be resolved. Regardless of the approach taken, a link between the mass in stars and the resulting stellar feedback budget must be made. Because individual stars are not resolved in the schemes described above, this relationship is obtained by averaging over the statistical distribution of stellar masses.

This distribution is given by the initial mass function (IMF). Combining an IMF with a set of stellar evolution models can produce the net feedback properties (e.g. SN rate, luminosity in various bands relevant to feedback, wind power and mass loss rate etc.) for a single stellar population (SSP) under the assumption that the IMF is fully sampled. Then, the feedback budget can be determined for a star particle in a simulation (typically with a dependence on its age and metallicity via lookup tables), rescaled by its mass. We will refer to this as IMF averaged feedback throughout this work. It is important to note that even when IMF averaged SN rates are used, SNe can still be modelled as discrete events by stochastically sampling the rates (see e.g. [Stinson et al. 2010](#); [Hopkins et al. 2014](#); [Kimm et al. 2015](#); [Revaz et al. 2016](#); [Smith et al. 2018](#)). Consistent evidence for a universal IMF has been amassed from observations of large populations of stars, featuring a steep power law at high masses ([Salpeter 1955](#)) with a knee at  $\sim 1 M_\odot$  ([Kroupa et al. 1993](#); [Kroupa 2001](#); [Chabrier 2003](#)). Potential deviations away from the universal IMF can arise in two forms. Firstly, there has been some evidence that the IMF may vary systematically between galaxies ([Hoversten & Glazebrook 2008](#); [van Dokkum & Conroy 2010](#); [Cappellari et al. 2012](#); [Conroy & van Dokkum 2012](#); [Kalirai et al. 2013](#); [La Barbera et al. 2013](#); [Geha et al. 2013](#)), with possible correlations with central velocity dispersion and/or metallicity. However, the magnitude of this phenomenon remains unclear. Nonetheless, if the IMF does indeed vary systematically, this effect is conceptually simple to include in IMF averaged feedback schemes. For example, in cosmological zoom-in simulations of Milky Way-like galaxies, [Gutcke & Springel \(2019\)](#) use an IMF that varies as a function of metallicity to adjust SN rates and metal enrichment from AGB winds on-the-fly.

Alternatively, deviations could arise due to variations

of the IMF on small scales or as a result of undersampling a universal IMF in small populations. The total distribution of stars in a galaxy is a composite of the various individual star forming regions. Thus, an integrated galactic IMF (IGIMF) arises from the combination of the IMF within individual star clusters and the cluster mass function ([Kroupa & Weidner 2003](#)). If a common universal IMF is well traced within each cluster independent of cluster mass, then the IGIMF will be identical to the universal IMF. If the IMF varies from cluster to cluster the shape of the IGIMF will change. In particular, if the high-mass cutoff is a function of cluster mass, then the IGIMF slope will be steeper than the universal IMF. There is evidence that massive stars are rarer in low-SFR environments ([Meurer et al. 2009](#); [Lee et al. 2009, 2016](#); [Gunawardhana et al. 2011](#)), which could be a consequence of this scenario. It has been posited that this could arise due differences in how star formation proceeds in clusters of different mass, leading to an intrinsic relationship between cluster mass and high-mass cutoff ([Kroupa & Weidner 2003](#); [Weidner & Kroupa 2006](#); [Weidner et al. 2010, 2013](#)). However, it has also been argued that no such deterministic link exists and that observations are consistent with a stochastically sampled uniform IMF ([Elmegreen 2006](#); [Corbelli et al. 2009](#); [Calzetti et al. 2010](#); [Fumagalli et al. 2011](#); [Andrews et al. 2013, 2014](#)). These effects cannot be captured a priori with IMF averaged feedback as they emerge as a result of stochastic effects arising from undersampling of the IMF in a given small population of stars.

The alternative is to populate star particles at their birth with an inventory of stars by explicitly sampling the IMF. Feedback budgets can then be based on the individual stars residing in the star particle. When star particles are massive enough, this will converge with the IMF averaged approach because the IMF will be well sampled within the particle. Taking the opposite limit yields the modelling of individual stars. The assumption that a stellar population samples the IMF well only holds for population masses above  $\sim 10^5 M_\odot$  ([Carigi & Hernandez 2008](#); [Revaz et al. 2016](#)), below which stochastic effects will begin to emerge. Explicit sampling of the IMF allows issues related to undersampling of the IMF (as described in the previous paragraph) to be captured. It also allows the inhomogeneous distribution of stellar feedback among stars (varying luminosities, mass loss, SN energy injection etc.) to be resolved. Various schemes for explicit IMF sampling have been presented and used in simulations of individual GMCs, patches of discs (stratified boxes) and entire galaxies (see e.g. [Gatto et al. 2017](#); [Sormani et al. 2017](#); [Geen et al. 2018](#); [Hu et al. 2017](#); [Hu 2019](#); [Fujimoto et al. 2018](#); [Emerick et al. 2019](#); [Applebaum et al. 2020](#); [Gutcke et al. 2020](#), some of which we will discuss in greater detail in Section 2).

[Su et al. \(2018\)](#) estimate the effect of using stochastically sampled stellar masses compared to IMF averaged feedback in cosmological zoom-in simulations. They find that as long as SNe are modelled as discrete events (even if sampled from IMF averaged rates), stochastic variation of the stellar content of star particles does not produce a significant departure from simulations run with IMF averaged feedback. However, they do not explicitly perform IMF sampling, instead using a toy model to modulate their IMF averaged feedback (OB winds, luminosities and SN rates). In Section 4 we will discuss the validity of such an approach. [Grudić &](#)

Hopkins (2019) use a similar technique in simulations of individual GMCs, but find that approximating the inhomogeneous distribution of UV luminosities among stars, leading to the presence of rare, bright sources, results in lower star formation efficiencies compared to using IMF averaged feedback. In non-cosmological simulations of dwarfs, Applebaum et al. (2020) find that when SN feedback and  $H_2$  dissociating radiation are linked to explicitly sampled stellar masses rather than being based on IMF averaged rates (that still discretize SNe), feedback is moderately less efficient at regulating SFRs and the mass of cold gas. We will discuss their findings in more detail in Section 4.

This work is laid out as follows. Section 2 contains an extended discussion of the details of explicit IMF sampling schemes. We shall use some simple Monte Carlo numerical experiments to demonstrate the advantages and disadvantages of several schemes, populating star particles of various masses. In Section 3 we use high resolution non-cosmological simulations of dwarf galaxies to directly compare the use of IMF averaged feedback to explicit IMF sampling. In Section 4 we discuss our findings and their consequences in greater detail, as well as providing a comparison to some other relevant works. Section 5 presents our conclusions. Appendix A demonstrates that our simulations are robust to stochastic effects by rerunning the early stages of a subset of our simulations with randomly perturbed initial conditions and different random number generator seeds.

## 2 POPULATING STAR PARTICLES FROM AN IMF

### 2.1 Requirements of an IMF sampling scheme

One of the main reasons for paying close attention to details of the output IMF in a galaxy formation simulation is its relationship to the feedback budget. Since the vast majority of stellar feedback arises from comparatively rare, massive stars, subtle changes to the distribution of stellar masses can potentially influence the evolution of the galaxy. When designing a scheme to populate star particles created in a galaxy formation simulation with stellar masses drawn from an IMF, there are two main requirements that are often in tension with each other. The scheme must attempt to reproduce the input IMF as closely as possible, but it should also conserve stellar mass. Problems arise because a sequence of discrete stellar masses drawn from an IMF is in general unlikely to sum exactly to a previously specified value (e.g. the mass of a star particle), with the last sampled mass overshooting the target. What a scheme does in this scenario determines how closely it prioritizes mass conservation vs. reproducing the IMF.

One possible solution is to accept the last draw and source more mass to make up the difference. Such an approach is trivial to implement if the initial star particle mass is smaller than the mass of the gas resolution element from which it is formed. Otherwise, the mass reservoir can be ‘topped up’ by taking mass from other nearby gas particles/cells (either by merging or partially draining them, see e.g. Hirai et al. 2020; Gutcke et al. 2020). If done in combination with the standard method for forming star particles (stochastically sampling the SFRs of individual gas particles/cells independently to trigger the spawning of or conversion to a star particle), care must be taken to avoid or

minimize inconsistencies between the expected SFR of the gas and the rate at which stellar mass is created (e.g. Hu 2019 avoids this issue by exchanging mass between star particles *after* they have been created). However, in this work we will avoid any additional transfer of mass to particles and focus on methods to populate a star particle of fixed mass with stars, presenting a scheme that can be easily incorporated into any existing implementation of star formation.

Before proceeding, we will comment on why it is important that an input IMF is accurately reproduced in a galaxy formation simulation. In nature, the IMF is an emergent property of the process of star formation, arising from the small scale physics governing the fragmentation and gravitational collapse of turbulent, star forming gas and its interaction with feedback. By contrast, in galaxy formation simulations it is impossible to resolve the physical processes that give rise to the IMF. An IMF must therefore be imposed upon the simulation as a sub-grid model, either in an explicit manner by sampling from it on-the-fly or by taking IMF averaged approaches to stellar feedback. The chosen IMF may be derived empirically from observations or it can be based on theoretical expectations. It can be a fixed, universal IMF or it could take a more complicated form, being allowed to vary with galactic or even local properties. Regardless of the form adopted, once chosen, the input IMF encodes the unresolved physics of small scale star formation that cannot be captured in the simulation. Therefore, it is imperative that it is not subsequently biased by numerical issues originating from the implementation. As an obvious example, when the star particle mass resolution begins to approach (or even drop below) the upper mass cut of the IMF, the resulting distribution of stellar masses is very vulnerable to being biased away from input IMF (as we shall show below). Such a bias must be avoided as much as possible, since it is obvious that the distribution should be independent of the mass resolution as this is entirely numerical.

A more subtle problem can occur in regions of low SFR. When a star particle is created and is populated from the IMF, it is possible that there is not enough mass in the local star forming cloud (let alone the star particle) to satisfy a draw from the input IMF. It is tempting under these circumstances to simply discard the draw, since it is clear that such a massive star could not form in this environment. However, this also leads to a biasing of the input IMF that has its basis in numerics not physics. If the resolved physics of the simulation frequently provides situations where there is not enough gas mass available to accurately sample from the input IMF, this suggests that the input IMF is inappropriate. A better IMF should be chosen that encodes either an empirical or theoretical model for how star formation proceeds in low SFR environments. If draws are discarded, then the resulting distribution of stellar masses is simply a flawed realisation of the input IMF rather than reflecting any resolved physics. One could imagine that in the scenario described above, a different output from the random number generator could have resulted in the massive star being formed later in the evolution of the star forming cloud, when there was sufficient mass available. It is also possible that the manner in which the cloud assembled is sensitive to resolution. The final distribution of stellar masses averaged over many star particles should have no such dependence on numerics since this introduces a bias with no physical basis.

Additionally, we note that it is entirely possible that a low mass galaxy does not form enough stars to fully populate the IMF. This does not necessarily indicate that the input IMF is inappropriate, rather that multiple realisations of the simulation should be performed to assess the impact of stochasticity.

In the previous discussion, it is clear that the majority of cases in which the output IMF can be biased are due to issues of mass conservation. While we have described why simply throwing away a draw from the IMF because of the lack of stellar mass must be avoided, it is also apparent that simply accepting every draw would result in a net overproduction of stars because the target mass will always be exceeded. An IMF sampling scheme must therefore balance the competing demands of mass conservation and IMF preservation. The compromise usually takes the form of an inconsistency between the target mass and the mass of the samples (which we will refer to as the assigned mass) on a particle by particle basis, but a consistency when averaged over many particles. The particle level inconsistency may be eliminated after the fact by a transfer of mass (as mentioned at the beginning of this section) or can simply be left as a mismatch between the dynamical and assigned mass of the particle (the approach we adopt in this work). Because the exact N-body interactions between stars cannot usually be treated in a galaxy formation simulation (the use of softened gravitational forces often being adopted) this inconsistency is not of much concern from a dynamical perspective. The mass inconsistency can also be resolved conceptually if low mass stars (which do not contribute substantially to the feedback budget) are not tracked explicitly. The mass inconsistency can then be thought of as a simple redistribution of the low mass stars between star particles, as long as the overall inconsistency sums to zero over many particles (e.g. [Applebaum et al. 2020](#) use this philosophy). This has no practical impact on the operation of the scheme, other than to rationalise the discrepancy. Additionally, it obviously does not work in the case where the combined mass of the explicitly tracked massive stars exceeds the dynamical mass. Regardless, if the inconsistency is too large there may not be sufficient mass to return via stellar winds and SN ejecta as required by the assigned stellar masses. We will briefly touch on this subject later in this work.

Finally, we note that we have been vague as to distinguishing between a truly universal IMF versus an IGIMF arising from an IMF that varies between clusters, as described in Section 1. For example, if stars born in clusters follow the shape of a universal IMF, but properties of the cluster (most importantly the mass) impose a high mass cutoff then the IGIMF (which is composed of the sum of the IMFs of the individual clusters) will be steeper than the canonical IMF ([Kroupa & Weidner 2003](#)). This means that the IGIMF will have a dependence on the mass function of the star forming regions with galaxy properties (mass, metallicity etc.) playing a key role. However, it is important to note that star particles should not be conflated with physical star clusters. Unless the adopted star formation prescription produces a distribution of star particle masses such that the mass function is an emergent property of the simulation (and is believed to be an accurate representation of the true cluster mass function), the star particle mass has no physical meaning. In almost all cases the star particle

mass is set uniformly as a parameter of the simulation or as a consequence of the gas resolution. This means that truncation of the upper end of a universal IMF based on the star particle mass is unphysical. If the use of a particular form of a cluster mass dependent IMF (and resulting IGIMF) is required, a more complex sub-grid model is needed.

## 2.2 Methods for explicit IMF sampling

We will now explore several methods for populating star particles with stellar masses from the IMF. As explained in the previous paragraph, we do not consider methods that account for the truncation of the high mass end of the IMF as a function of the desired total sample mass (the target mass) (e.g. the ‘sorted sampling’ method of [Weidner & Kroupa 2006](#)) as in general star particles do not accurately represent stellar clusters. Three simple methods of sampling from the IMF to reach a target mass are ‘stop before’, ‘stop after’ and ‘stop nearest’ (see [Haas & Anders 2010](#)). These terms refer to what is done with the last drawn stellar mass which will inevitably exceed the desired target.

‘Stop before’ sampling discards the last drawn stellar mass. It guarantees that the total drawn stellar mass (which we refer to as the assigned mass,  $m_{\text{asn}}$ ) will not exceed the mass of the star particle. However, this means that the sum of assigned masses over all particles will inevitably show a deficit relative to the total dynamical mass of star particles formed. It will also create a bias towards low mass stars since a high mass star is more likely to exceed the target mass. The output IMF will therefore deviate downwards from the input IMF, being finally truncated at the star particle mass. As the star particle mass is increased, this bias is reduced. Likewise, the fractional deficit of the total assigned mass to the total particle mass will reduce because the relative contribution of the last draw is reduced. ‘Stop after’ sampling takes the opposite approach, always keeping the last drawn star. By avoiding discarding any draw, this method guarantees that the distribution of assigned stellar masses perfectly follows the shape of the input IMF. The downside is that this comes at the cost of normalizing the IMF upwards, always assigning more stars to particles than the available stellar mass. Again, the relative impact of this bias is reduced as the star particle mass is increased. It should also be noted that any scheme which accepts the last drawn star and then makes the sampled and dynamical masses consistent by taking additional mass from nearby gas *after* the decision to create a particle has already been made will suffer a similar bias, artificially inflating the local SFR.

A compromise between these two methods is the ‘stop nearest’ approach. With this scheme, the last drawn stellar mass is kept if the total assigned mass is closer to the target mass with its inclusion than without. The motivation is that the cases of the last drawn mass being discarded will be counterbalanced by the occasions it is kept. This is true for large star particle masses, where the size of the gap between the penultimate drawn mass and the target mass is insignificant compared to the target mass. However, as we shall demonstrate, this method suffers from the same biases as the ‘stop before’ scheme (albeit to a lesser extent) when the star particle mass is smaller.

A common deficiency of these three methods is that the populations of individual particles are completely inde-



pendent of each other. This is only appropriate if the star particle represents an independent single stellar population (SSP) (e.g. as formed in a star cluster). It is inappropriate for small star particle masses since the ensemble of star particles represent the stellar population together. However, as discussed earlier, it is usually impossible at the resolutions of a galaxy formation simulation for a realistic population of stars to be an emergent feature of the local physical environment. Thus, in order to accurately recover an input IMF, each star particle cannot be populated in isolation. Instead, information about the distribution of stellar masses in previous star particles must be taken into account to correct for biases. We implement this requirement in a scheme we refer to as ‘adjusted target’. Fig. 1 contains a flowchart detailing the algorithm. The scheme is similar to ‘stop after’ except that the target mass is not in general the same as the particle mass. Instead, the target mass for a given particle is adjusted based on how far the previous star particle overshoot its target. This allows us to keep the total assigned mass consistent with the total stellar mass formed across many particles, but to simultaneously perfectly reproduce the input IMF because we never discard a draw. This scheme is very similar to that presented in Hu et al. (2017) with the difference that we do not adjust the dynamical mass of particles to enforce consistency between assigned mass and dynamical mass for each particle individually. This avoids unphysical mass transfer over potentially arbitrary distances.<sup>1</sup> Similarly, there is no inter-particle mass exchange so it has the advantage that it can be trivially implemented on top of any pre-existing implementation of star formation with a minimum of additional coding.

When a star particle is populated, we draw stellar masses from the input IMF and assign them to the star particle until the total assigned mass exceeds the target. The last draw is kept and the star particle is now finished with. The ‘offset mass’ is equal to the sum of masses assigned to the particle minus the target. The target mass of the next particle to be populated is set to its particle mass minus the offset mass from the previous particle. The target mass will always be equal to or less than the particle mass. However, while the assigned stellar mass will always exceed the target mass it will not always exceed the particle mass. Some particles will have an excess of assigned stellar mass while others will have a deficit. Averaged across multiple star particles the total assigned mass will equal the total star particle dynamical mass.

Without modification, the algorithm presented in Fig. 1 accounts for circumstances where the target mass is negative or zero. This occurs if the last assigned stellar mass of the previous particle resulted in a substantial overshoot of the target. When the target mass is negative or zero, the algorithm will draw no stellar masses for the star particle and the offset mass is reduced by the mass of the star particle, resulting in a higher target mass for the next star particle. This feature of the adjusted target scheme means that it is possible to include stellar masses that are larger than the fiducial star particle mass, simply resulting in a particle that has more assigned mass than dynamical mass and

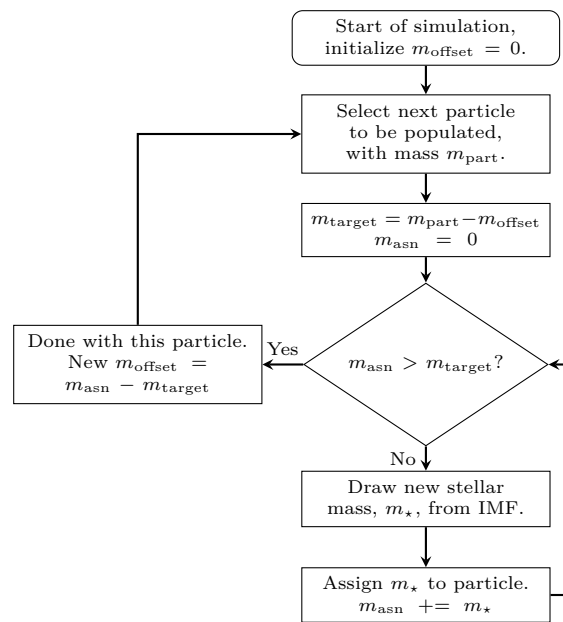


**Figure 1.** A schematic illustration of our ‘adjusted target’ star particle populating scheme. Stellar masses are drawn from the input IMF until a target mass is exceeded. The last drawn mass is always kept, ensuring that the output IMF is unbiased. The target mass is not in general equal to the dynamical mass of the star particle, but compensates for the amount that the target was overshoot when sampling the previous star particle (the offset mass). Thus, some star particles will have more assigned stellar mass than their dynamical mass while the reverse is true for others. Across an ensemble of star particles the total assigned mass is equal to the total dynamical mass and the input IMF is perfectly reproduced.

some particles that compensate by having no assigned mass. For example, consider the extreme example where a  $100 M_{\odot}$  star is the first draw for a  $20 M_{\odot}$  star particle and, for the sake of simplicity, the current offset mass is  $0 M_{\odot}$  (meaning that the target mass for this star particle is also  $20 M_{\odot}$ ). The draw of the  $100 M_{\odot}$  star is accepted and assigned to the star particle. The target mass has been exceeded, so sampling is now concluded for this star particle. The offset mass is now  $80 M_{\odot}$  because the target was overshoot by that amount. The algorithm will produce target masses for the next four  $20 M_{\odot}$  particles that are less than or equal to zero. They will therefore have no assigned stellar mass. The resulting total assigned mass equals the total dynamical mass across the five particles, at the cost that each particle has an inconsistency between its individual assigned and dynamical masses. As mentioned above, because we cannot anyway resolve the dynamics of individual stars this is largely irrelevant. It is only a problem if there is not enough mass available to be returned through feedback (discussed below). In practice, cases such as this are rare because high mass stars are proportionally less likely to be drawn. However, as we shall demonstrate, failing to allow for their formation biases the IMF and reduces the overall feedback budget. The target mass usually stays close to the particle mass (unless the particle mass is considerably smaller than typical stellar

<sup>1</sup> The scheme of Hu (2019) addresses this issue, but involves the additional complications of mass transfer between star particles.

mass), only moving substantially if a very massive star is drawn.

As described here, our algorithm only ensures the input IMF is reproduced over the sequence of sampled star particles. It does not account for spatial information, so it does not guarantee that a sub-volume of a simulation will contain a population of stars that reproduce the IMF. In principle, multiple concurrent realisations of the underlying “book-keeping” can be used. For example, in a cosmological simulation it would make sense to define the “next star particle” as the next formed in the same galaxy, maintaining separate offset masses for individual systems, ensuring that the IMF is maintained in each. For a non-cosmological simulation the galaxy could likewise be divided into separate regions where the algorithm is applied independently, maintaining the IMF locally. However, in practice we find that this is unnecessary since it is extremely unlikely that applying the algorithm globally results in, for example, all the massive stars being formed at one side of the galaxy. A regional division may be necessary if an input IMF that has a dependence on local conditions is used such that IMF varies strongly within a galaxy at a given moment in time. If the IMF varies slowly as a function of time (compared to the time-scale on which  $m_{\text{offset}}$  fluctuates,  $\sim m_{\text{part}}/\dot{M}_*$ ) and remains relatively uniform within a galaxy then this is not necessary. It should also be noted that our scheme as proposed does not permit the spatial clustering of stars as a function of their mass to be directly specified, with correlations simply arising from completely random sampling of the IMF, although this is unlikely to be of much concern at the resolution of global galaxy simulations.

Finally, we will briefly mention some other sampling methods that have been used in the literature that do not populate a star particle with a sequence of drawn stellar masses. In stratified box simulations, [Gatto et al. \(2017\)](#) populate sink particles with stellar masses drawn from the IMF. They only consider massive stars, sampling once from a mass range of  $9 - 120 M_{\odot}$  every time  $120 M_{\odot}$  is accreted onto the sink and assume the remaining mass forms lower mass stars. However, this scheme can produce an overall deficit of massive stars because sink particle masses are not in general a multiple of  $120 M_{\odot}$ . [Geen et al. \(2018\)](#) adopt a similar approach in simulations of GMCs. [Sormani et al. \(2017\)](#) present a scheme which instead divides the IMF into a number of bins and populates particles by performing Poisson sampling to determine the number of stars in each bin based on the expected number. This has the advantage of reproducing the IMF in an unbiased, albeit discretized, form across an ensemble of particles, at the cost of a discrepancy between the sampled and dynamical mass within a given particle. No additional correction is necessary to ensure the discrepancy sums to zero over a population of particles (in contrast to the adjusted target scheme), but the individual discrepancies can in theory be much larger than the previously described schemes (although increasingly large discrepancies represent more unlikely outcomes of the sampling). The discretized nature of the [Sormani et al. \(2017\)](#) scheme means that it incurs a penalty to computational cost when sampling and increasing memory requirements when the IMF is sampled at finer granularity (i.e. smaller mass bins), a problem not faced by other schemes in this section which allow for a continuum of stellar masses.

### 2.3 Monte Carlo tests of IMF sampling methods

We now present some idealized Monte Carlo tests of the four main IMF sampling schemes described in the previous section (stop before, stop after, stop nearest and adjusted target) to demonstrate their properties when used to populate star particles. Throughout this work we will use a [Kroupa \(2001\)](#) IMF with minimum and maximum stellar masses of  $m_{\text{min}} = 0.08 M_{\odot}$  and  $m_{\text{max}} = 100 M_{\odot}$ , respectively. Our findings will hold in a qualitative sense for any reasonable input IMF. We will draw samples from the IMF for a total mass budget of  $10^7 M_{\odot}$ . We have confirmed that this is a sufficiently large amount of mass that it can be populated almost perfectly with stellar masses drawn from our input IMF (no matter what method is used) if no restrictions are applied. However, we will instead subdivide this mass reservoir into particles of mass  $m_{\text{part}}$  and use the four IMF sampling methods to populate them. This is representative of how star particles would be populated in a galaxy formation simulation. We will use various values of  $m_{\text{part}}$  to examine the resolution dependence of the four schemes.

In Fig. 2 we compare the total distribution of individual stellar masses across the various star particles to the analytic expectation from the input IMF. Specifically, we show the number of stars per logarithmic mass bin,  $\xi_L = dN/d\log_{10} m_*$ . In the top panels we show  $\xi_L$  directly while in the bottom panels we show its ratio to the analytic expectation from the input IMF. The general trends are as follows. The stop before method results in a suppression of the high-mass end of the IMF while boosting the low-mass end, as expected. The maximum stellar mass that can be accepted with the stop before method is equal to the star particle mass, since any higher mass will carry it over the total. Even then, this is only true when it is the first mass drawn for the particle. In general, because a more massive star is more likely to carry the total assigned mass over the star particle mass than a less massive star, low mass draws are more likely to be accepted. When  $m_{\text{part}} = 20 M_{\odot}$ , the shape of the output IMF is very distorted. There is a  $\sim 15\%$  enhancement of  $\xi_L$  for stars less than  $\sim 0.5 M_{\odot}$ , followed by a sharp drop at higher masses with a net suppression above  $3 M_{\odot}$ . The biasing effect is less severe as  $m_{\text{part}}$  is increased because the relative importance of the final drawn stellar mass is reduced. However, there is still a strong suppression of the high-mass end of the IMF when  $m_{\text{part}} = 100 M_{\odot}$  and it is still noticeable when  $m_{\text{part}} = 500 M_{\odot}$ .

The stop after method always perfectly reproduces the shape of the input IMF (modulo some noise at the high-mass end) because no draw is ever discarded. However, this always results in an overshoot of the particle mass meaning that the absolute number of stars is biased upwards. When  $m_{\text{part}} = 20 M_{\odot}$ , this manifests as an enhancement of  $\xi_L$  by an average of  $16\%$  across the whole mass range. Again, this bias reduces as the particle mass increases, with an enhancement of  $3.9\%$  and  $0.8\%$  when  $m_{\text{part}}$  is increased to  $100 M_{\odot}$  and  $500 M_{\odot}$ , respectively.

The stop nearest method suffers from the same issues as the stop before method, albeit to a lesser extent. In this method, a draw will be rejected if the drawn mass is more than twice as large as the gap between the current total assigned mass and the particle mass. It therefore also enhances the low-mass end of the IMF while suppressing the

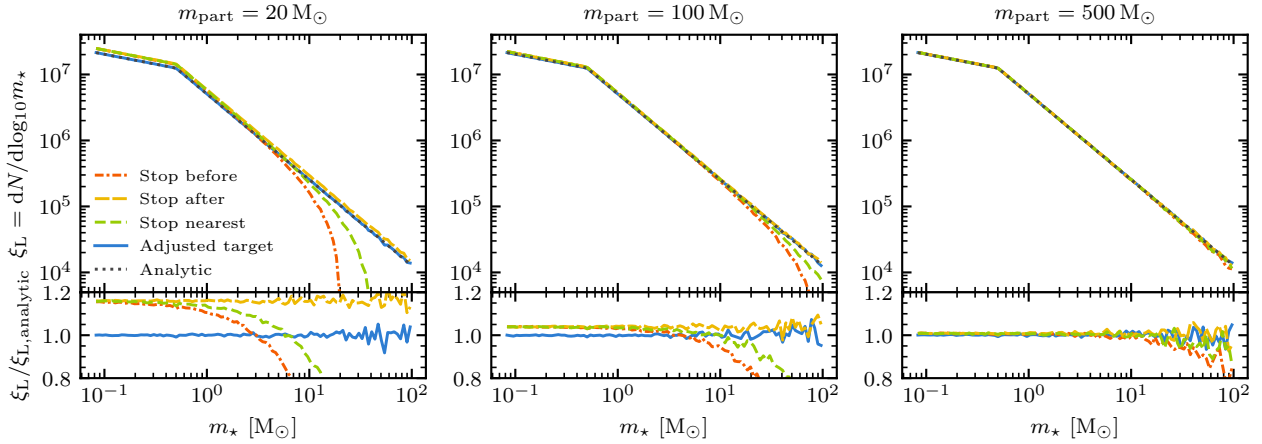


**Figure 2.** The distribution of individual stellar masses when a mass budget of  $10^7 M_\odot$  is divided into particles of mass  $m_{\text{part}}$  which are then populated using one of the four sampling methods described in the main text. The top panels show the absolute distribution while the bottom panels show the distributions relative to the analytic expectation. Both the stop before and stop nearest methods bias the low-mass end of the IMF up and suppress the high-mass end. The stop after method preserves the shape of the input IMF but results in a larger normalization across the whole mass range. These biases become less pronounced for larger  $m_{\text{part}}$ . The adjusted target scheme reproduces the input IMF for all  $m_{\text{part}}$ .

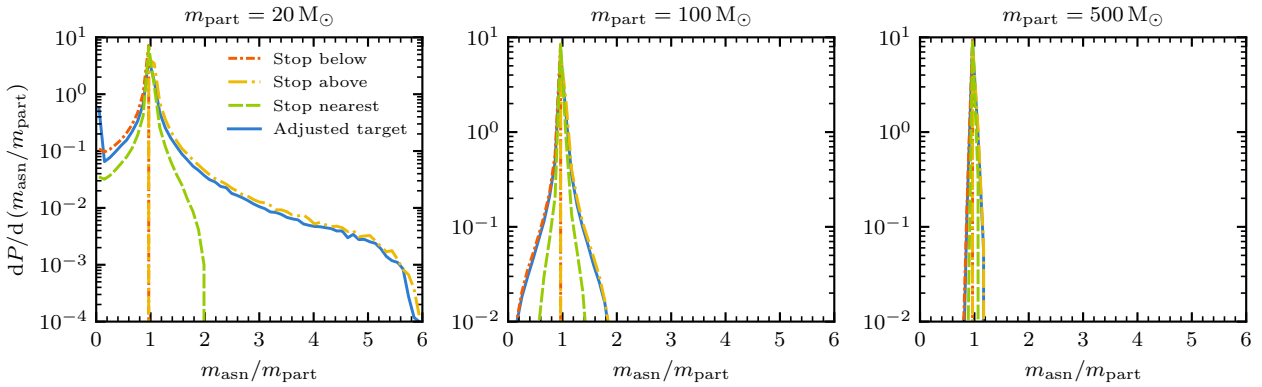


**Figure 3.** PDFs of  $m_{\text{asn}}/m_{\text{part}}$  for individual particles populated with stars using the four sampling methods. All schemes produce a peak at unity i.e. where the assigned mass is completely consistent with the particle mass. Stop before and stop have tails above and below unity, as expected, indicating particles where the assigned mass has under- or overshot, respectively. The stop nearest scheme provides a tighter PDF. The adjusted target scheme essentially traces the wings of the stop before and stop after schemes. The relative scatter about unity decreases as  $m_{\text{part}}$  is increased.

high-mass end, although not as much as the stop before scheme. Again, this bias is most pronounced at low particle masses and is only marginally apparent (but still present) when  $m_{\text{part}} = 500 M_\odot$ . Finally, Fig. 2 shows that the population across all star particles is highly consistent with the input IMF when the adjusted target scheme is used, independent of star particle mass. It reproduces the shape and normalization almost perfectly, with only slight variation at the high-mass end due to noise (since those stars are rare). The amplitude of the noise is the same as when the total  $10^7 M_\odot$  is sampled monolithically (not shown).

As described in previous sections, IMF sampling schemes must balance preserving the input IMF with the two additional issues of minimizing the inconsistency between the assigned and dynamical masses for each individual star particle and conserving mass across the population of star particles. First, we shall examine the relative mass inconsistency,  $m_{\text{asn}}/m_{\text{part}}$ , for the individual star particles

populated in our Monte Carlo experiments. Fig. 3 shows PDFs for this ratio for our four trialed sampling methods with  $m_{\text{part}} = 20 M_\odot$ ,  $100 M_\odot$  and  $500 M_\odot$ . All distributions peak at a value of 1 i.e. where the assigned mass is consistent with the particle mass. The stop before has a tail that extends to lower values of the ratio i.e. representing particles that have less assigned mass than their particle mass. The reverse is true for stop after. These trends are an obvious result of the construction of the schemes. The stop before scheme can assign no more mass than  $m_{\text{part}}$  and no less mass than  $\text{MAX}(m_{\text{part}} - m_{\text{max}}, 0)$ . Equivalently, the stop after scheme can assign no less mass than  $m_{\text{part}}$  and no more mass than  $m_{\text{part}} + m_{\text{max}}$ . These limits can be seen in the PDFs and result in a narrowing of the distribution as  $m_{\text{part}}$  is increased.

The stop nearest method results in the tightest distribution of  $m_{\text{asn}}/m_{\text{part}}$  about unity of the four schemes. It is possible for the assigned mass to be below or above

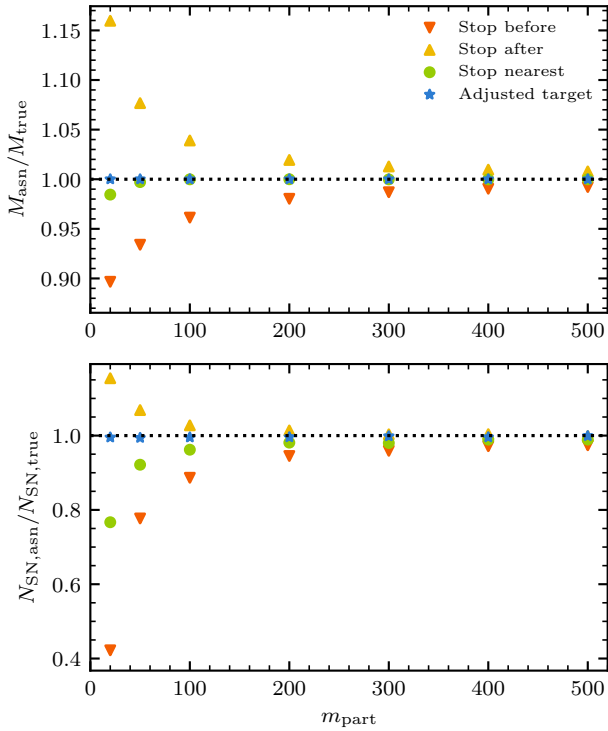


**Figure 4.** Top: Ratio between the total assigned mass and total star particle mass across the entire population of particles for various particle masses,  $m_{\text{part}}$ , and the four different sampling methods. Bottom: the total number of SN progenitors in the populations relative to that predicted by the input IMF, assuming stars in the mass range  $8 - 35 M_{\odot}$  produce core-collapse SNe. Only the adjusted target scheme can produce a total mass in assigned stars that is consistent with the star particle mass for  $m_{\text{part}}$  as low as  $20 M_{\odot}$ . It is also unique in producing the correct number of SNe progenitors for all  $m_{\text{part}}$ . The stop nearest approach has a deficit in the number of SN progenitors at low  $m_{\text{part}}$  but converges to the correct value by  $m_{\text{part}} = 500 M_{\odot}$ .

the particle mass. The minimum mass that can be assigned is  $\text{MAX}(m_{\text{part}} - \frac{1}{2}m_{\text{max}}, 0)$  while the maximum mass that can be assigned is  $\text{MIN}(2m_{\text{part}}, m_{\text{part}} + \frac{1}{2}m_{\text{max}})$ . Again, the distribution tightens in a relative sense as  $m_{\text{part}}$  increases because the impact of the last drawn stellar mass is reduced. The adjusted target scheme has the largest spread in  $m_{\text{asn}}/m_{\text{part}}$  of the four schemes. It too can assign more or less stellar mass than the particle mass. Its minimum assignable mass is the same as the minimum for the stop before scheme and its maximum assignable mass is the same as the maximum for the stop after scheme. It can be seen in Fig. 3 that the wings of the adjusted target PDFs trace those of the stop before and stop after PDFs. However, when  $m_{\text{part}} = 20 M_{\odot}$ , adjusted target produces more particles with no assigned mass (relative to stop before and stop nearest) because there will occasionally be a series of  $m_{\text{asn}} = 0$  particles to compensate for a massive star being drawn previously (as described in the previous section).

Fig. 4 shows how the choice of sampling scheme affects the ratio between the total assigned mass for the whole ensemble of particles,  $M_{\text{asn}} = \sum_j m_{\text{asn},j}$ , and the true mass

budget,  $M_{\text{true}} = 10^7 M_{\odot}$ , for various values of  $m_{\text{part}}$ . As expected, the stop before scheme produces a deficit of assigned stellar masses (because it always throws away the last draw) while stop after correspondingly produces an excess (because it always keeps the last draw). This is most apparent at low values of  $m_{\text{part}}$ , but a small bias is still evident at  $m_{\text{part}} = 500 M_{\odot}$ . Stop nearest has a marginal mass deficit at the lowest  $m_{\text{part}}$  but recovers the true mass by  $m_{\text{part}} = 100 M_{\odot}$ . The adjusted target always recovers the true mass budget even with  $m_{\text{part}} = 20 M_{\odot}$ . Of particular relevance to galaxy formation simulations is whether the total stellar feedback budget is recovered. Because the majority of the budget is generated by massive stars, the recovery of the amount of feedback per unit stellar mass from the input IMF is sensitive to how closely a sampling scheme reproduces the high-mass end of the IMF. In Fig. 4 we also show how the total number of SN progenitors generated by our Monte Carlo experiments compares to the expected number. We assume that stellar masses in the range  $8 - 35 M_{\odot}$  will produce core collapse SNe (we ignore Type Ia SNe). Again, as expected, the stop before and stop after schemes produce too few or too many SN progenitors, respectively, relative to the analytic expectation. The stop nearest scheme also produces too few SN progenitors with deficits of 23.8%, 7.8% and 3.8% for  $m_{\text{part}} = 20 M_{\odot}$ ,  $50 M_{\odot}$  and  $100 M_{\odot}$ , respectively. It converges onto the correct number of progenitors within 1% for  $500 M_{\odot}$ . By contrast, the adjusted target scheme gives the correct number of SN progenitors within 0.5% or better across all the values of  $m_{\text{part}}$  we test. Note that if the maximum core collapse SNe progenitor mass is increased, the biasing of the feedback budget will be worse. Likewise, feedback channels that depend strongly on the most massive stars (e.g. ionizing radiation) will show similar biases.

To summarise, the stop before, stop after and stop nearest sampling methods all fail to reproduce the input IMF except at large star particle masses. This has direct consequences for the stellar feedback budget, resulting in substantial under- or overestimation of the number of SN progenitors when  $m_{\text{part}}$  is less than  $\sim 100 M_{\odot}$ . By contrast, the adjusted target scheme does not bias the input IMF in any way, produces a total assigned mass that is consistent with the total star particle mass and recovers the correct feedback budget. The sole advantage of the stop nearest method is that it is the best scheme for minimizing the discrepancy between the assigned and dynamical mass of an individual particle. However, this discrepancy is not particularly important as galaxy formation simulations cannot typically resolve exact N-body dynamics and the much larger inconsistency with the input IMF and the total stellar mass budget is a far worse penalty. Above  $m_{\text{part}} = 500 M_{\odot}$  the schemes largely converge, so in this mass range the stop nearest approach may be adopted simply because it can be implemented locally to each task in a parallel computation. However, implementing our improved scheme is not substantially more complex and carries negligible additional computational penalty. Our scheme can be integrated into any pre-existing star formation scheme that uses star particles with a minimum of effort because it does not require additional modification of the mass of star particles or the transfer of mass between star particles.



### 3 EXPLICIT IMF SAMPLING VS. IMF AVERAGING IN SIMULATIONS

In this section we will study the impact on galaxy evolution simulations of using explicit IMF sampling to determine the stellar feedback budgets of star particles as opposed to the more common IMF averaged approach. We will present simulations of an idealized isolated dwarf galaxy with a baryonic mass resolution of  $20 M_{\odot}$ . We include stellar feedback in the form of SNe, photoionization and photoheating in H II regions and photoelectric heating of dust grains. Detailed descriptions of these models can be found in [Smith et al. \(2020\)](#) (hereafter [Paper I](#)), but we will summarise the salient details in the following section. For convenience, we will denote simulations with SNe, ionizing radiation and photoelectric heating by the abbreviations *SN*, *PI* and *PE*, respectively. Simulations with all feedback channels switched on are denoted as *SN-PI-PE* while *NoFB* is adopted when no feedback is used. We will refer to simulations that explicitly sample the IMF by the abbreviation ‘*IMFsam*’ and simulations that use IMF averaged stellar feedback as ‘*IMFav*’. The *IMFsam* simulations were originally presented in [Paper I](#).

#### 3.1 Numerical methods

We use the moving-mesh code AREPO ([Springel 2010](#); [Pakmor et al. 2016](#)) along with our own sub-grid models for star formation and stellar feedback (which are described in more detail in [Paper I](#)). We use the GRACKLE chemistry and cooling library<sup>2</sup> ([Smith et al. 2017](#)) in its primordial six-species non-equilibrium mode, along with tabulated metal cooling, ionization and heating from a meta-galactic UV background ([Haardt & Madau 2012](#)) and the self-shielding prescription of [Rahmati et al. \(2013\)](#). Gas cells can have a non-zero SFR when their Jeans mass drops below 8 times the cell mass. The SFR is then given by a simple Schmidt law,  $\dot{\rho}_{\star} = \epsilon_{\text{SF}} \rho / t_{\text{ff}}$ , where  $\rho$  is the gas density,  $t_{\text{ff}} = \sqrt{3\pi/32G\rho}$  is the local free-fall time and we adopt a fixed efficiency of  $\epsilon_{\text{SF}} = 0.02$ , motivated by observed efficiencies in dense gas (see e.g. [Krumholz & Tan 2007](#), and references therein). The SFR is then stochastically sampled to convert gas cells into collisionless star particles.

We include photoelectric heating of dust grains by a spatially varying far-UV (FUV) field generated by star particles. The FUV energy density at each location in the domain is calculated using the gravity tree to sum the fluxes from sources, using a local approximation for attenuation by dust which is valid in dust-poor systems. We approximate the dust-to-gas ratio as a function of metallicity using the broken power-law of [Rémy-Ruyer et al. \(2014\)](#). H II regions around ionizing sources are included using a novel anisotropic overlapping Strömgren type approximation (first presented in [Paper I](#)). The balance between the ionizing photon luminosity and the recombination rate is calculated in independent angular pixels around sources to determine the extent of an H II. This helps mitigate the mass-biasing error encountered by previous methods. The algorithm accounts for H II regions from multiple sources overlapping. If a cell is tagged as belonging to an H II region, it is immediately heated to  $10^4$  K and is forbidden from cooling below that temperature while it remains tagged. SN feedback is included with the

scheme first presented in [Smith et al. \(2018\)](#). This injects mass, metals, energy and momentum into the gas cell containing a star particle and its immediate neighbours (those that share a face with the host cell). The scheme ensures an isotropic injection of feedback quantities which is non-trivial in a Lagrangian code. We use the SN scheme in its mechanical feedback mode which compensates for missing momentum when the Sedov-Taylor phase of a SN remnant is unresolved. In practice, at the resolution we adopt in this work the majority of SNe are well resolved and we find that we achieve similar results when a simple thermal dump of SN energy is used. In this work, we do not include stellar winds.

When the explicit IMF sampling scheme is used (*IMFsam*), star particles are populated with an inventory of stellar masses at the moment of creation using the adjusted target scheme described in Section 2. Rejection sampling is used to draw stellar masses from the IMF. We use a single value of the offset mass for the whole galaxy at any one time, rather than concurrent versions for different regions of the galaxy (see the discussion in Section 2.2).<sup>3</sup> We do not explicitly record the masses of stars less than  $5 M_{\odot}$  since they would contribute negligible feedback (as we do not include winds from AGB stars), although they are taken into account for the purposes of determining the total stellar mass assigned to the star particle. For stars more massive than  $5 M_{\odot}$ , we then use lookup tables as a function of mass in order to determine quantities relevant to feedback. We make the simplifying assumption in this work that all stars have a metallicity of  $0.1 Z_{\odot}$ , the initial metallicity of our initial conditions. None of the quantities used have a strong dependence on metallicity relative to the deviation from the initial metallicity that we see in this work, so this approximation is reasonable. We obtain the lifetime of the star from the PARSEC grid of stellar tracks ([Bressan et al. 2012](#)). The FUV and ionizing photon luminosities of the star are derived from the OSTAR2002 grid of stellar models [Lanz & Hubeny \(2003\)](#) as compiled by [Emerick et al. \(2019\)](#), making the approximation that they are fixed at their main sequence values throughout the life of the star. The net luminosity of a star particle is the sum of all extant stars assigned to it. When a star reaches the end of its life it ceases to contribute radiation. Star particles with extant massive stars have their time-steps limited to 0.1 Myr, although in practice their time-step is usually much smaller as constrained by other criteria. If a star in the mass range  $8 - 35 M_{\odot}$  reaches the end of its life, a SN is triggered, resolved from the host star particle. The ejecta mass and metallicity depends on the progenitor mass, based on [Chieffi & Limongi \(2004\)](#). We use a constant SN energy of  $10^{51}$  ergs for all SNe. When SN feedback is switched off, we still return ejecta when a SN progenitor reaches the end of its life but do not inject the energy.

For simulations using IMF averaged feedback quantities

<sup>2</sup> <https://grackle.readthedocs.io>

<sup>3</sup> Our simulations are parallelised using MPI, so an effort must be made to synchronize the sampling between tasks (i.e. there must be a well defined order of star particle sampling). In practice, we find the simplest and most computationally efficient way to achieve this is to perform all sampling on a single MPI rank with the resulting inventories distributed back to the ranks on which the star particles reside.

(*IMFav*) the sampling procedure is not performed. Instead, lookup tables of FUV and ionizing photon luminosities, and SN rates per unit stellar mass as a function of population age are used. For consistency, these tables are derived using the same relationships between individual stellar mass and feedback quantities that are used in the *IMFsam* schemes. We begin by populating a  $10^8 M_\odot$  SSP with stellar masses drawn from the IMF, the high mass guaranteeing that the IMF is very well sampled. Lifetimes and luminosities are obtained in a similar manner to the on-the-fly approach used in the *IMFsam* schemes. We then integrate through the lifetime of the SSP, recording how the net FUV and ionizing photon luminosities decrease as stars reach the end of their lives. We also obtain SN rates by recording when stars in the  $8 - 35 M_\odot$  mass range die. We then normalize these luminosities and rates by the initial mass of the SSP. When a simulation is performed, star particles are assigned their luminosities using these lookup tables based on their age. The expected number of SNe that will be produced by a star particle in a given time-step,  $\Delta t$ , is

$$\bar{N}_{\text{SN}} = \dot{n}_{\text{SN}}(t_{\text{part}}) m_{\text{part},0} \Delta t, \quad (1)$$

where  $\dot{n}_{\text{SN}}(t_{\text{part}})$  is the SN rate per unit mass obtained from the lookup tables as function of star particle age and  $m_{\text{part},0}$  is the initial star particle mass at the point of creation, before mass loss due to feedback. The SN rate is normalized by  $m_{\text{part},0}$  rather than  $m_{\text{part}}$  in order to recover the normalization used when creating the rate tables from the SSP. In other words, SNe are independent events representing an implicit sampling of the IMF and so the chances of a SN being generated from a star particle should not be reduced because a previous SN occurred and reduced the mass of the particle. Likewise, luminosities obtained from the lookup tables are normalized by the initial particle mass, not the current mass. In constructing the IMF averaged luminosities we have already explicitly linked the radiation output to the initial mass of the SSP and it is therefore independent of the SN events that have occurred in the star particle and the ensuing mass loss. The number of SNe that occur in a given time-step is then determined by drawing from a Poisson distribution with a mean  $\lambda = \bar{N}_{\text{SN}}$ . In Section 4 we will discuss in more detail why Poisson sampling is the appropriate procedure. If a SN occurs, we map the age of the star particle back onto the mass of the progenitor to obtain the ejecta mass and metallicity. Like the *IMFsam* schemes, star particles have a maximum time-step of 0.1 Myr enforced. This ensures the changes of luminosity are time-resolved, but also guarantees that  $\bar{N}_{\text{SN}} \ll 1$ . This is necessary to ensure that SNe are individually time-resolved, which is important to accurately capture clustering effects.

It is possible that a star particle may not have sufficient mass to return as ejecta for a triggered SN event. For the *IMFsam* scheme this is a result of the potential discrepancy between the assigned and dynamical mass of the star particle. For the *IMFav* scheme this is because the stochastic sampling of the rates means that it is possible, albeit unlikely, for a single star particle to produce more SNe than its mass should allow. If there is insufficient mass in a star particle to return as ejecta, we instead return as much as possible (i.e. the mass of the particle) and remove the particle. As reported in Paper I, this is a relatively rare occurrence and results in an overall reduction of the total ejecta

across all SNe by 5.1% for a  $20 M_\odot$  star particle. Only 2% of SNe have their ejecta mass reduced by more than 30% and none have their ejecta reduced by more than 36%. This may be of concern if a detailed study of chemical enrichment is of interest (ignoring uncertainties in yields) but for this work we find this level of deviation from the tabulated yields acceptable. It is also possible that in the event of an entire star particle being removed due to a lack of ejecta mass another massive star hosted in the particle is prematurely deleted before it has reached the end of its life. This occurs in less than 0.1% of the SN events in our simulations.

### 3.2 Simulation details

For our idealized dwarf galaxy we use the ‘fiducial’ initial conditions from Paper I, generated using the MAKE-NEWDISK code (Springel et al. 2005). The system has a virial mass of  $10^{10} M_\odot$ . There is a  $6.825 \times 10^7 M_\odot$  gas disk with an exponential radial density profile with a scale length of 1.1 kpc. The vertical structure is set to achieve hydrostatic equilibrium at an initial temperature of  $10^4$  K. The gas is initialized with a metallicity of  $0.1 Z_\odot$ . We do not include a circumgalactic medium (CGM). There is also an initial stellar disk with a mass of  $9.75 \times 10^6 M_\odot$  and the same radial density profile as the gas disk. The vertical structure is Gaussian with a scale height of 0.7 kpc. Star particles present in the initial conditions do not contribute stellar feedback. The rest of the mass of the system is in the form of a live, spherically symmetric dark matter halo. This follows a Hernquist (1990) density profile chosen to provide a close match to a Navarro et al. (1997) profile with a concentration parameter,  $c$ , of 15 and a spin parameter,  $\lambda$ , of 0.04. Gas cells and star particles have a mass of  $20 M_\odot$  (derefinement and refinement operations keep the gas cells within a factor of 2 of this target mass), while dark matter particles have a mass of  $1640 M_\odot$ . Gravitational softening lengths are fixed at 1.75 pc and 20 pc for star and dark matter particles, respectively. Gas cells use adaptive softening lengths down to a minimum of 1.75 pc. The initial conditions are relaxed for 100 Myr with cooling but without star formation while initial turbulence is driven with a pseudo-SN feedback scheme (described in detail Paper I). This is to avoid a rapid vertical collapse of the disk when the simulations are started.

### 3.3 Results

Fig. 5 shows the SFR for the simulations, averaged over 10 Myr. Dashed lines show results from simulations with IMF averaged feedback (*IMFav*) while solid lines show simulations with explicit IMF sampling (*IMFsam*). This convention is used throughout this work. Without feedback, the SFR rises rapidly and is only limited by the supply of gas (we only perform an *IMFsam NoFB* simulation). When feedback is included, the results are qualitatively the same between *IMFav* and *IMFsam* simulations. A detailed discussion about how the various feedback schemes regulate the SFR can be found in Paper I. As found in that paper, photoelectric heating by itself is inefficient, providing little suppression of star formation. It is slightly more efficient in the *IMFsam* simulation, reducing the peak SFR reached, but this is an extremely marginal effect. SN feedback is able to suppress the SFR by almost two orders of magnitude on average. It does so in a very bursty manner. The *IMFav* and *IMFsam* produce near identical results. Differences between

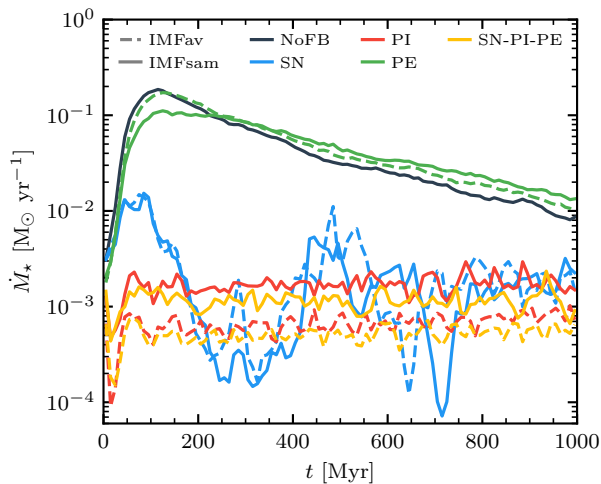


**Figure 5.** SFRs for our simulations, averaged over 10 Myr. Simulations without feedback or with photoelectric heating alone result in a high SFR limited only by the available gas supply. SN feedback regulates SF in a bursty manner with IMF averaging (*IMFav*) and explicit IMF sampling (*IMFsam*) giving essentially identical results. Photoionization feedback is also able to regulate star formation. However, it is more efficient by a factor of 2.4 in *IMFav* compared to *IMFsam*.

the two are well within the margin of numerical noise arising from stochastic sampling/trigging of SNe. We confirm this in Appendix A, where we repeat the early stages of these simulations four additional times with different seeds for the random number generators and with randomly perturbed initial conditions.

Photoionization feedback is also able to regulate SFRs (see Paper I for a detailed discussion of why this occurs). It produces a smoother SF history as it disrupts star forming regions locally in a more gentle manner. When averaged over the last 500 Myr of the simulation (allowing the initial transient to settle), the *IMFsam* simulation regulates the SFR to roughly the same degree as the SN feedback simulations. However, the *IMFav* reduces the SFR by a factor of 2.4 relative to the *IMFsam* simulation. When all feedback channels are turned on (*SN-PI-PE*) with explicit IMF sampling, SFRs are reduced by  $\sim 40\%$  relative to the SN or photoionization only simulations, but this is small compared to the initial reduction from the no feedback case. When the IMF averaged values are used instead, switching on all the feedback results in a reduction of 26% relative to the *IMFav* PI simulation but 73% relative to the *IMFav* SN simulation. Photoionization is therefore the dominant regulator of star formation in the *IMFav* simulations, in contrast to the *IMFsam* case where we observe parity. The relative difference between the strength of photoionization feedback between the *IMFav* and *IMFsam* is not a stochastic effect, as can be seen in Appendix A.

Fig. 6 shows PDFs for the ambient density where star particles are created and where SNe occur<sup>4</sup>. We exclude

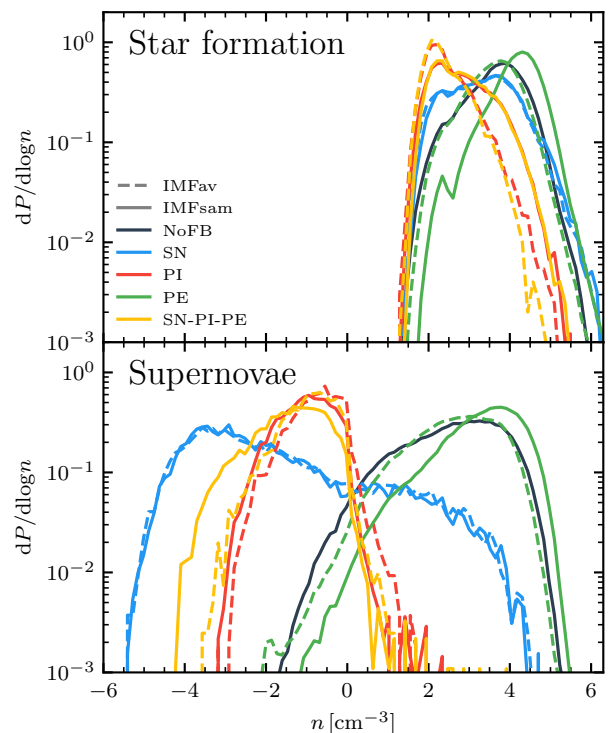


**Figure 6.** PDFs of the ambient density where star particles are created (top) and SNe explode (or would explode if SN feedback was switched on) (bottom), ignoring the first 400 Myr. SNe broaden the distribution of birth densities. Ionizing radiation shifts the peak to lower densities as it prevents the collapse of gas to high densities. This effect is more pronounced in the *IMFav* simulations. When SNe are the only source of feedback, SNe explode over a broad range of densities as dense clouds are dispersed and superbubbles are created. *IMFav* and *IMFsam* give identical results. When ionizing radiation is included, dense gas is dispersed prior to SNe occurring but the growth of superbubbles is restricted, preventing the low density tail from extending as far. It extends slightly further in *IMFsam* SN-PI-PE because the effect of ionizing radiation is not as strong.

the first 400 Myr to ignore the initial transient phase of the simulation. Our Jeans mass based star formation criteria means that the onset of star formation occurs between  $\sim 20 - 100 \text{ cm}^{-3}$ . Simulations without feedback or with photoelectric heating alone peak at around a density of  $10^4 \text{ cm}^{-3}$  as gas continues to collapse beyond the onset of star formation. The difference between the *IMFav* and *IMFsam* photoelectric heating runs is simply a result of the different gas fractions in the disk due to the offset in SFR peaks in the first 400 Myr, essentially producing an offset of the disk evolution in time. When SN feedback is used alone, the PDF of star formation ambient densities is broadened. This is because the feedback alters the distribution of dense gas by driving turbulence and disrupting collapsing clouds. *IMFav* and *IMFsam* give identical PDFs. When ionizing radiation is included the peak of the distribution is moved to lower densities and the maximum density reached is reduced. This

<sup>4</sup> In simulations where SN feedback is switched off, we still record where SNe would occur either based on a SN progenitor reaching the end of its life (in the *IMFsam* simulations) or by sampling

the SN rates (in the *IMFav* simulations). As noted in Section 3.1 we also return ejecta mass but do not add SN energy.



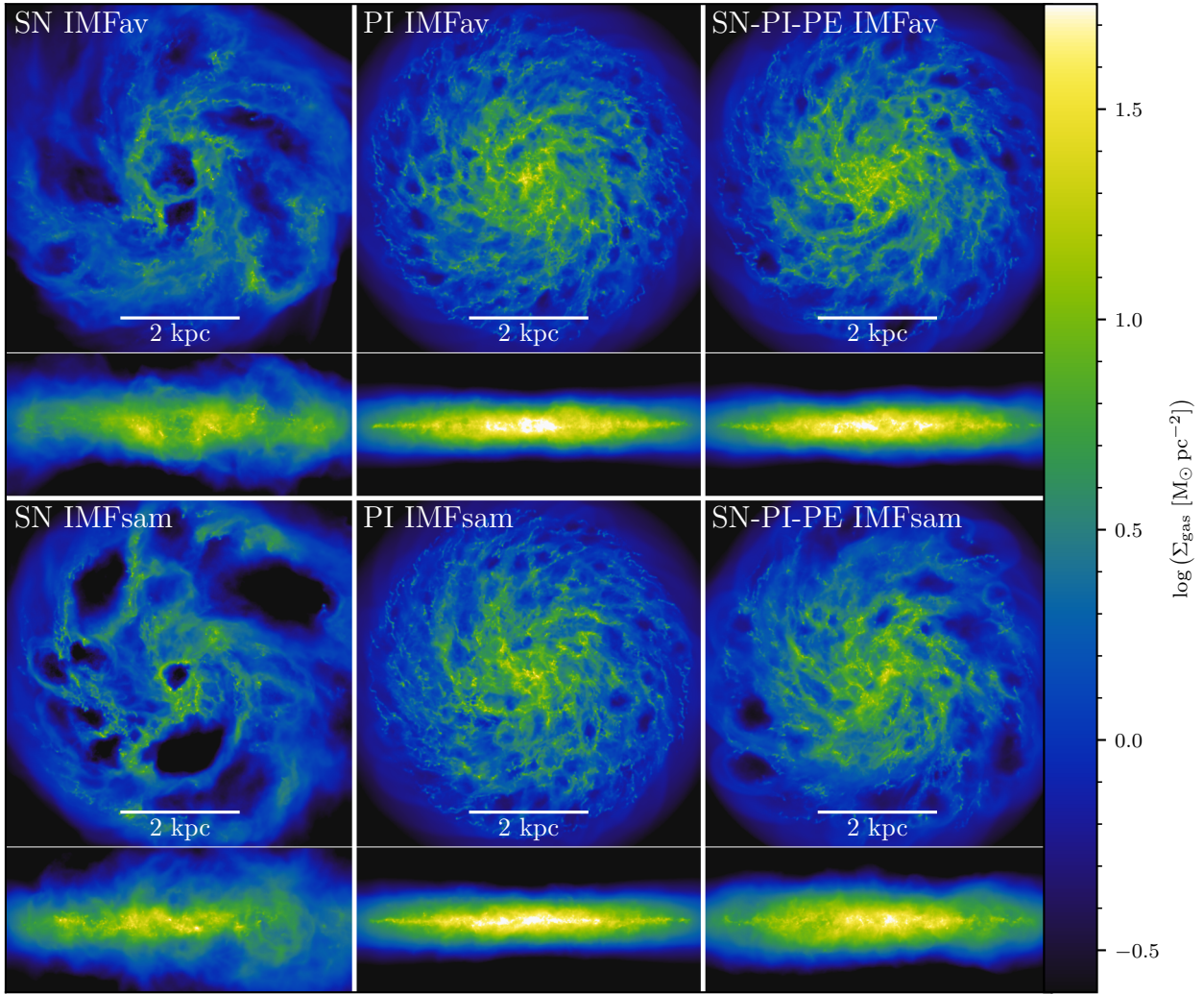


**Figure 7.** Face-on and edge-on projections of the gas disks at 1 Gyr. *NoFB* and *PE* simulations are not shown. SN feedback alone produces a thick and highly disordered disk, with large transient cavities caused by SN superbubbles. When ionizing radiation is the only source of feedback the disks are more ordered and the large holes are not evident. The *SN-PI-PE IMFav* simulation is qualitatively the same as the *PI IMFav* run, but when explicit IMF sampling is used small, transient SN-driven cavities appear marginally more frequently.

is because the radiation is able to halt the collapse of dense clouds and disrupt them earlier than the SN feedback (which is delayed by the lifetime of its progenitors). It can be seen that this effect is significantly more pronounced in the *IMFav* than the *IMFsam* simulations, a key difference between the two methods.

In the absence of feedback or with photoelectric heating alone, the PDFs of the ambient density where SN progenitors die reflects the PDFs of star particle birth densities with a broadening towards lower densities. This lower density tail arises because of runaway gas consumption in star forming clouds, dropping the local density, as well as being caused by star particles drifting out of their (now very compact) birth clouds. When SN feedback is used alone, the PDF of SN site densities spans roughly ten orders of magnitude in density. The first SNe to occur in a star forming cloud explode in the dense gas of star forming regions. They are able to disperse these dense clouds and successive SNe contribute

to the creation of a superbubble, with each subsequent SN occurring in lower density gas. This gives rise to the broad range of ambient densities. Again, the simulation using IMF averaged SN rates and that explicitly sampling the IMF for SN progenitors produce essentially identical PDFs. When ionizing radiation is included (either on its own or with the other feedback channels) almost no SNe occur in star forming gas. The radiation is able to clear dense gas prior to SNe occurring. The PDFs are similar for the *IMFav* and *IMFsam* simulations. The low density tail does not extend as far as the SN only simulations. This is because the creation of superbubbles is inhibited by the ionizing radiation acting to reduce the clustering of SNe, as shown in greater detail in [Paper I](#). The *SN-PI-PE IMFsam* PDF extends to slightly lower densities than the *IMFav* equivalent because the impact of the radiation on clustering is not as strong in this case, allowing some SNe to occur in larger bubbles.

Fig. 7 shows face-on and edge-on projections of the gas



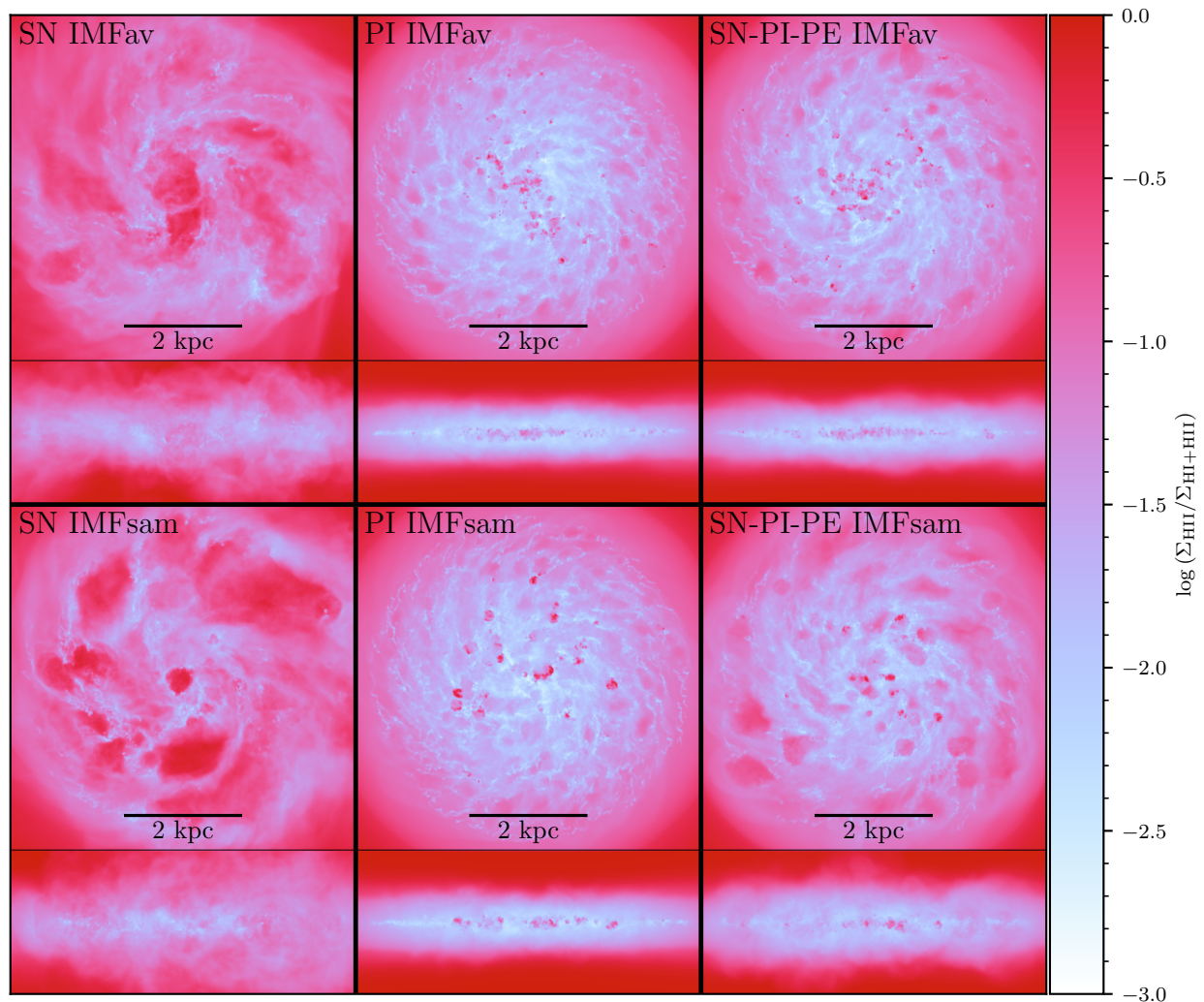


**Figure 8.** The surface density of H II divided by the total hydrogen density at 1 Gyr, shown face-on and edge-on. *NoFB* and *PE* simulations are not shown. Generally, the ionized regions trace the low density gas. Patches of high ionization fraction can be seen embedded in dense gas in the simulations with photoionization feedback. These are H II regions around ionizing sources. The *IMFav* simulations produces many small H II regions scattered throughout the disk compared to the *IMFsam* approach which features rarer, but larger H II regions.

disk after 1 Gyr. Simulations *NoFB* and *PE* are not shown, but equivalent plots can be found in [Paper I](#). In these simulations a large proportion of the gas has been consumed by 1 Gyr, leaving isolated, extremely compact knots of dense gas within a low density ambient medium. The gas disks in those simulations are extremely thin. For the simulations that we do show in [Fig. 7](#), the *IMFav* and *IMFsam* simulations are qualitatively similar. When SNe are the only source of feedback, the disk is thick and highly disordered. SNe superbubbles blow transient holes in the disk, with star formation restricted to the remaining dense structures. When ionizing radiation is the only source of feedback, the disk lacks the large holes and is more regular. There is a complex filamentary structure, with dense star forming clouds embedded in lower density gas. The disk is not as thick as the *SN* simulations, but it has not collapsed vertically as in the *NoFB* and *PE* simulations. The simulations with all feedback channels switched on are qualitatively similar to the *PI*

simulations, particularly in the *IMFav* case. However, the *SN-PI-PE IMFsam* simulation produces small, SN-driven cavities more regularly than the *IMFav* equivalent.

[Fig 8](#) shows the ratio between ionized and total hydrogen surface densities, face-on and edge-on. It is therefore a form of projected ionization fraction. With reference to [Fig. 7](#), it can be seen that ionized regions largely trace the diffuse gas. However, in the simulations with photoionization feedback there are small regions of high ionization fraction embedded in dense gas. These are H II regions around ionizing sources. There is a qualitative difference in the distribution and size of H II regions between the *IMFav* and *IMFsam* simulations. The former simulations contain many small H II regions, speckled throughout the disk. The *IMFsam* simulations produce fewer, but larger H II regions. This difference is not a transient effect and persists throughout the course of the simulations.

The reason for this difference lies in the properties of

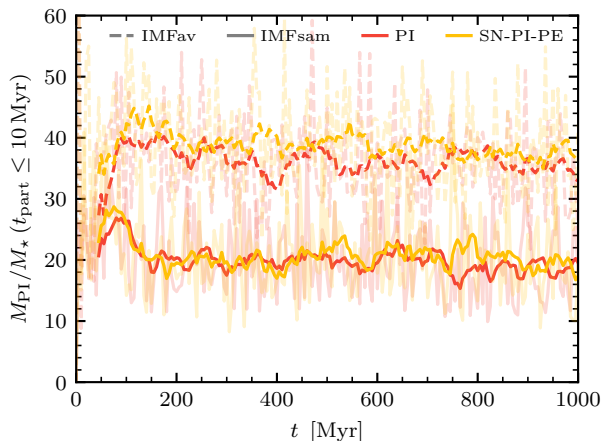


**Figure 9.** The mass of gas tagged as belonging to an H II region normalized by the mass in young stars. The instantaneous value (shown in the paler colours) is very noisy so we also plot a 50 Myr moving average (the bold colours). The *IMFav* simulations produce almost twice as much photoionized gas per unit stellar mass as the *IMFsam* equivalents.

the ionizing sources when IMF averages are used as opposed to explicitly tracking the emission from individual massive stars. With the former approach, every star particle of the same age emits the same ionizing flux. However, the *IMFsam* scheme correctly ties the origin of ionizing photons to comparatively rare, bright sources. The total luminosity of ionizing radiation per unit stellar mass is the same in both methods, by construction. However, the distribution of this luminosity between sources makes a significant difference to the ability to photoionize gas. Despite having approximately half the average global SFR, the *IMFav* simulations with photoionization feedback keep roughly the same mass of gas photoionized as the *IMFsam* simulations. This is illustrated in Fig. 9 where we plot the ratio between the photoionized mass (tagged as belonging to an H II region by our sub-grid model) and the mass in star particles younger than 10 Myr. The pale lines show the instantaneous value at every output time (5 Myr) but as this is extremely noisy we also plot a 50 Myr moving average. Fig. 9 demonstrates that stars are almost twice as efficient at creating H II regions when the IMF averaged luminosities are assigned to star particles.

One might assume that if the net ionizing photon rate per unit stellar mass is the same in the different types of simulation they would be able to photoionize the same quantity of gas. However, the ionizing photon budget is dominated by rare, massive stars. With the *IMFav* average approach, every star particle is an ionizing source. A  $20 M_{\odot}$  star particle will initially produce ionizing photons at a rate of approximately  $10^{48} \text{ s}^{-1}$ , this rate only beginning to decrease after  $\sim 3$  Myr, corresponding to the lifetime of the most massive stars. It will be able to photoionize a  $20 M_{\odot}$  gas cell as long as the gas density is less dense than  $216 \text{ cm}^{-3}$ . It can be seen in Fig. 6 that a large fraction of star particles are born in gas lower than this density. Once even a small quantity of gas is photoionized, the resulting D-type expansion allows the source to grow an H II region. Additionally, because *every* star particle immediately begins emitting this radiation

upon creation, as soon as a star forming region creates a single star particle the further collapse of the cloud can begin to be arrested. This effect leads to the shifting of the birth density PDF towards the SF threshold in Fig. 6. By contrast, even though explicit IMF sampling leads to far brighter sources they are significantly rarer. An ionizing photon rate of  $10^{48} \text{ s}^{-1}$  corresponds roughly to a  $16 M_{\odot}$  star. Only 8% of  $20 M_{\odot}$  star particles are assigned at least one star more massive than  $16 M_{\odot}$  when the *IMFsam* scheme is used. This means that on average a proportionally larger amount of stellar mass has to be created before an ionizing source capable of affecting the star forming cloud is born, resulting in a higher effective cloud-scale star formation efficiency. This has the added effect that star forming clumps can collapse to higher densities, as seen in Fig. 6. The result is that a higher ionizing flux is required to photoionize the gas, raising the minimum mass for which a star can generate an H II region. This means that while the *IMFav* simulations produce many small H II regions around low brightness sources, the *IMFsam* simulations produce fewer, but larger, H II regions around massive stars. For the reasons explained above, the latter scenario is less efficient at regulating star formation.

## 4 DISCUSSION

We now discuss our findings in greater detail and place them in the context of some other relevant works. In Section 4.1 we review best practices for schemes that trigger discrete SNe from IMF averaged rates. We show that if SNe are the only form of feedback, this will yield identical results to explicit IMF sampling, which is what we see in our simulations. In Section 4.2 we discuss our contrasting result that the photoionization feedback *is* in fact sensitive to the choice of method. We consider what these findings might mean for other non-SN feedback channels and how this sensitivity depends on resolution. We also explore whether a simpler toy model can capture the effects produced by explicit IMF sampling.

### 4.1 Insensitivity of supernova feedback to IMF averaging vs IMF sampling

#### 4.1.1 Best practices for discretizing IMF averaged SN rates

Mac Low & McCray (1988) showed that as long as the number of SNe a star particle will produce over its lifetime is more than  $\sim 10$  then the injection of SN feedback can be modelled as a continuous injection of energy. However, at higher resolution resolving the effects of discrete SNe becomes important (see e.g. Su et al. 2018; Applebaum et al. 2020). Keller & Kruijssen (2020) also demonstrate that simply injecting the entire feedback budget of the star particle in one event also deviates from simulations that account for a spread of SN events as a function of time. The impact of SN feedback is highly dependent on the clustering properties of the SNe (Sharma et al. 2014; Yadav et al. 2017; Gentry et al. 2017, 2019; Fielding et al. 2017, 2018; El-Badry et al. 2019 and Paper I). It is therefore important that if explicit IMF sampling is not used SNe must still be modelled as individual events sampled from the IMF averaged SN rates (if the resolution is high enough to detect the effects).

After an expected number of SNe,  $\bar{N}_{\text{SN}}$ , that will occur in a given time-step has been determined from the SN rate (in general a function of star particle age and metallicity), *initial* particle mass and time-step size (as described in Section 3.1), there are two main approaches to converting these rates into discrete SN events. In the first approach, Bernoulli trials can be carried out every time-step to determine whether a SN occurs. This essentially represents the flipping of a biased coin. If  $\bar{N}_{\text{SN}} \leq 1$ , then a Bernoulli trial is carried out with a probability of success equal to  $\bar{N}_{\text{SN}}$  to decide whether a single SN occurs. If  $\bar{N}_{\text{SN}} > 1$ , then the number of SNe that occur is at least equal to the integer part of  $\bar{N}_{\text{SN}}$  with a Bernoulli trial carried out with a probability equal to the fractional part of  $\bar{N}_{\text{SN}}$  to determine whether an additional SN is added (see e.g. [Stinson et al. 2010](#) and the RIMFS scheme of [Revaz et al. 2016](#)). This approach enforces a relatively smooth sampling of the rates, implicitly assuming that SN events are spread out evenly through whatever interval was used to determine the SN rates in the first place. When star particle masses are small, it also implicitly assumes that massive stars are distributed evenly across the particles which is essentially equivalent to assuming that the IMF is well sampled in each particle. In other words, these schemes capture the mean SN rates but do not capture the noise that emerges when considering a truly random sampling of an IMF in a single star particle.<sup>5</sup>

Sampling from the Poisson distribution captures this noise. The probability of  $N_{\text{SN}}$  occurring given  $\bar{N}_{\text{SN}}$  is

$$P_{\text{Pois}}(k = N_{\text{SN}}) = \frac{\bar{N}_{\text{SN}}^k e^{-\bar{N}_{\text{SN}}}}{k!}. \quad (2)$$

Sampling from this distribution will produce a number of SN events that are scattered about  $\bar{N}_{\text{SN}}$ , capturing the noise, in contrast to the Bernoulli trial method.

It is worth pointing out that there is a great deal of confusion in the literature between conducting Bernoulli trials and sampling the binomial distribution, with the latter frequently being used when referring to the former.<sup>6</sup> The binomial distribution describes the probability of achieving a given number of successes from a finite number of independent Bernoulli trials that have the same probability of success. In the limit that the number of trials is one, the binomial distribution converges to the Bernoulli distribution, but this is a trivial statement. Alternatively, if multiple time-steps all have the same SN rate then the total number of SN produced across all the time-steps will represent a draw from the binomial distribution. But one cannot “sample from the binomial distribution” to produce a number of SNe given

an expected number of SNe for an individual star particle. This confusion also frequently leads to the statement that Bernoulli trial and Poisson sampling schemes are generally equivalent, because the binomial and Poisson distributions converge in the limit of many trials with low probability of success. This is true across many time-steps if  $\bar{N}_{\text{SN}}$  is sufficiently small *and* the SN rate does not change between each time-step. However, within each of the small time-steps the Bernoulli trial and the Poisson draw are only equivalent when  $\bar{N}_{\text{SN}}$  is very small such that  $P_{\text{Pois}}(N_{\text{SN}} > 1) \rightarrow 0$ , which is a subtly different convergence criterion. Thus, both schemes may produce the same number of SNe averaged over some long timescale, but the temporal clustering will be different, unless this criteria is met. In practice, this limit is frequently desirable because in order to correctly capture the effects of SN clustering we wish to treat SNe individually. However, it is still more formally correct to draw from a Poisson distribution (technically allowing for the possibility that more than one SNe occur in a given time-step) but impose a time-step limiter to ensure that  $\bar{N}_{\text{SN}}$  is very small such that it is extremely unlikely that more than one SNe occurs. That is the approach we take in this work.

#### 4.1.2 The equivalence of discretized SN rates and explicit IMF sampling

[Applebaum et al. \(2020\)](#) use simulations of an isolated  $M_{\text{vir}} = 10^9 M_{\odot}$  dwarf to directly compare an explicit IMF sampling feedback scheme to an IMF averaged scheme similar to ours. Having established elsewhere in the work (with cosmological zoom-in simulations) that continuous injection of SN energy results in a weaker impact of feedback, they discretize their SNe by sampling from the IMF averaged rates (which they refer to as ‘quantized feedback’). The feedback used is comprised of Type II SNe,  $\text{H}_2$  dissociating Lyman-Werner (LW) radiation, Type Ia SNe and stellar winds, although the latter two channels remain IMF averaged in all simulations. They find that the quantized feedback simulations result in 10% more star formation and 30% more cold ( $T < 1000 \text{ K}$ ) gas compared to simulations that use explicit IMF sampling. They posit two possible causes for this. The first is that the difference is being driven by the different distributions of LW sources between the two schemes. They suggest that this difference occurs because the SNe and dominant LW sources are co-spatial when explicit IMF sampling is used, but it could also be directly related to the presence of rarer, brighter sources with this method. The second suggestion is that sampling SNe from IMF averaged rates could produce a different clustering of SNe than the explicit sampling scheme. As we have already argued, this should not be the case if the schemes are constructed in a consistent manner. They carry out a Monte Carlo experiment to compare the timing of SNe produced from star particles that are populated with stars from the IMF as opposed to those that sample the IMF averaged SN rates. With their adopted particle mass of  $420 M_{\odot}$  and time-step of 1 Myr, they find that approximately 25% of particles will experience at least one time-step in which more than one SN occurs when the explicit IMF sampling is used. When they use Bernoulli trials to sample the rates this never happens (because  $\bar{N}_{\text{SN}}$  is always less than one). [Applebaum et al. \(2020\)](#) note that they could possibly have seen different results if they had adopted Poisson sampling instead of their Bernoulli trial scheme.

<sup>5</sup> Which may or may not be desirable, depending on the manner in which one believes the IMF to be sampled in nature. Nonetheless, it is inconsistent with the form of explicit IMF sampling presented in the majority of this work.

<sup>6</sup> This is because Bernoulli trials are sometimes referred to as binomial trials (as distinct from, but related to, the binomial distribution). Anecdotal evidence gathered by tracing such references back to the details of published methods papers or publicly available code, where available, suggests that references to sampling from a binomial distribution most likely always refer to a Bernoulli trial scheme. For clarity, we will consistently refer to Bernoulli trials in this work, even when citing authors that prefer the alternate phrasing.



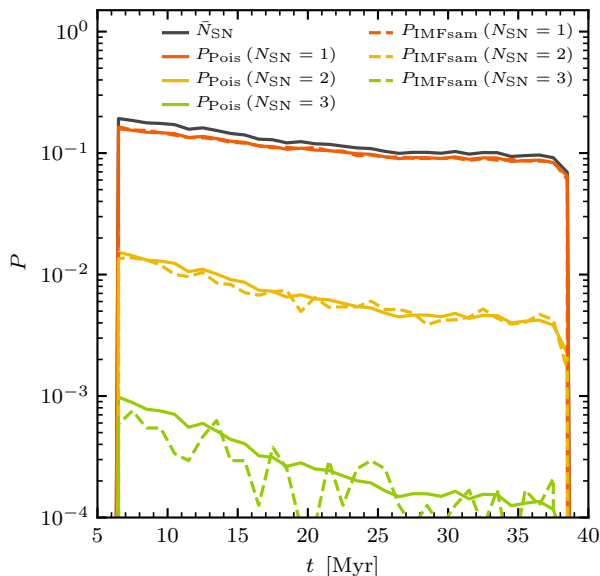


**Figure 10.** We demonstrate that for a  $420 M_{\odot}$  star particle with a time-step of 1 Myr (as used in [Applebaum et al. 2020](#)), the timing of SNe are well described by Poisson distributions. For each time-step in the life of the star particle, we plot the expected number of SNe,  $\bar{N}_{\text{SN}}$ , in black. This is also equivalent to the probability of triggering a single SNe when a simple Bernoulli trial scheme is used. The solid coloured lines show the probability of one, two or three SNe being produced in the time-step assuming a Poisson distribution with a mean of  $\bar{N}_{\text{SN}}$ . The dashed coloured lines show the equivalent probability derived from our Monte Carlo experiment, obtained as the fraction of particles that produce one, two or three SNe in the time-step when we explicitly populate particles with stellar masses drawn from the IMF. The total mass of particles is  $10^7 M_{\odot}$ . It can be seen that they follow Poisson distributions (although the  $N_{\text{SN}} = 3$  case is noisy due to the rarity of that number of SNe being produced).

When we repeat their experiment with Poisson sampling instead of Bernoulli trials, we find that the fraction of particles experiencing multiple SNe in a time-step is identical to the explicitly sampled IMF particles, to within 0.3%. Furthermore, we demonstrate in Fig. 10 that the SNe rates that emerge from the particles that are populated from the IMF are described very well by Poisson distributions. For a given 1 Myr time-step, we plot the expected number of SNe,  $\bar{N}_{\text{SN}}$ , and the probability that a particle will produce one, two or three SNe in that time-step, assuming a Poisson distribution with a mean of  $\bar{N}_{\text{SN}}$ . We over-plot (in dashed lines) the fraction of star particles from our Monte Carlo experiment (which total  $10^7 M_{\odot}$ ) that produce that number of SNe in that time-step. It can be seen that the two agree very well (although the  $N_{\text{SN}} = 3$  fractions are very noisy because of the rarity of such an event). Indeed, we find that the number of SNe in a time-step are well described by Poisson distributions whatever the choice of particle mass and time-step, in contrast to a Bernoulli trial scheme.

With star particles of mass  $420 M_{\odot}$ , a time-step of 1 Myr is too large for the Bernoulli trial approach to converge with the more consistent Poisson distribution. However, the discrepancy still appears to be relatively small. It is possible that the use of a ‘blast-wave feedback’ model ([Stinson et al.](#)

2006) exacerbates the effect since the adopted sub-grid evolution of the SN remnant (which affects the length of time for which cooling is shut off in this model) is different for a single injection of the energy of multiple SNe compared to spreading those events into multiple independent injections. Regardless, if the SN clustering is the primary cause of the difference between the quantized feedback and explicitly sampled IMF schemes, then it results from an inconsistent implementation of the SN rate sampling. We suspect that the difference is more likely to be caused by the first explanation (differences in the distribution of LW sources). Whatever the cause, we feel that the results of [Applebaum et al. \(2020\)](#) should only be interpreted as reinforcing the need for explicit IMF sampling when pre-SN feedback is included. They do not demonstrate that the stochastic sampling of IMF averaged SN rates is an inferior approach to explicit IMF sampling *in the absence* of pre-SN feedback channels.

The fact that the distribution and timing of SN events among star particles is identical when we use quantized feedback or explicit IMF sampling also shows that the stellar mass implied by the SN events is consistent with the dynamical mass to the same degree in both cases. Both quantized sampling of SN rates and explicit IMF sampling allow the fraction of star particle mass occupied by low mass stars to vary, by construction. Some particles will have more massive stars per unit stellar mass than the IMF average, while others have correspondingly fewer. However, in the case of quantized sampling of SN rates, the inventory of the star particle is not known until a SN occurs, indicating that a SN progenitor implicitly existed in the particle from its birth. This means that it is impossible for the level of non-SN feedback (which will also be pre-SN) generated by the star particle to be made consistent with the stellar inventory that is ‘discovered’ once SNe have occurred. This can be thought of as an inconsistency between the implied distributions of stellar masses responsible for the SN and non-SN feedback (see [Applebaum et al. 2020](#), fig. 3 for an illustration of this effect). With explicit IMF sampling, the stellar inventory is known from the birth of the particle, so the level of pre-SN feedback can be made consistent with the number and timing of the SNe produced by the particle. In the absence of non-SN feedback, quantized SN feedback and explicit IMF sampling are equivalent.

To summarise this section, we find that if SNe are the only source of stellar feedback, triggering discrete, individual SNe from IMF averaged rates gives identical results to explicit sampling of the IMF at the moment of a star particle’s creation (assuming the sampling can be carried out without biasing the IMF, as described in Section 2.2). We caution that this is only the case when the time-step in which the sampling is carried out is sufficiently small and that, in general, sampling from a Poisson distribution is the correct procedure. We have demonstrated this with our simulations shown in Section 3.3 but have described in this section why this must necessarily be true for any consistently constructed scheme. Therefore, if SNe are the only form of stellar feedback considered in a simulation nothing is gained by adopting an explicit IMF sampling scheme, which carries with it a penalty in terms of code complexity and (potentially) memory requirements.



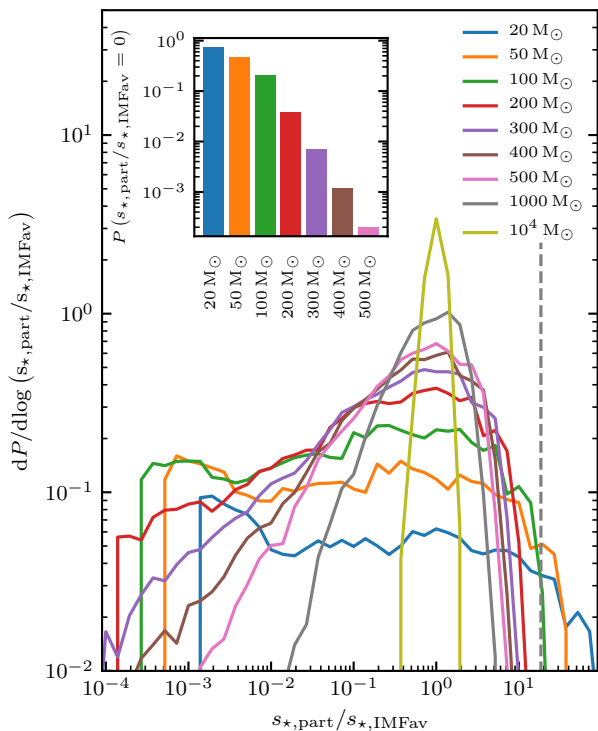


**Figure 11.** The distribution of the specific ionizing photon rate, normalized by the IMF average, for  $10^7 M_\odot$  of stellar mass divided into star particles and populated from the IMF using the adjusted target scheme. The lines show PDFs for different particle masses for those particles that have non-zero ionizing luminosities, while the inset plot shows the fraction of particles that have not been assigned a star that produces ionizing photons. The smaller the particle mass, the larger the spread about the IMF averaged value. The vertical dashed line indicates the maximum physical value for our adopted stellar mass range, corresponding to a  $100 M_\odot$  star. High resolution particles can exceed this specific ionizing photon rate if they have been assigned a more massive star than their dynamical mass, but as discussed in the main text, this does not result in over-bright sources.

## 4.2 Sensitivity of non-supernova feedback to IMF sampling

### 4.2.1 Under what circumstances does the sensitivity arise?

SN feedback is unique among stellar feedback channels in that it is composed of discrete, instantaneous (relative to other astrophysical timescales) events. All other forms of stellar feedback (e.g. radiation or stellar winds) are more continuous in nature, coupling to gas over an extended period of time. The degree to which the impact of the feedback is sensitive to the details of IMF sampling depends on the resolution in two ways. Firstly, does explicit IMF sampling produce significant enough inhomogeneities from particle to particle for results to deviate from an IMF averaged approach? The larger the star particle mass, the smaller the spread in feedback properties. Secondly, is the gas resolution high enough that the difference causes a resolvable effect? This also depends on other simulation details, such as the star formation prescription.

In the simulations we presented in this work, the pre-

dominant difference between the *IMFav* and *IMFsam* simulations was the efficiency of the photoionization feedback. We can study how the level of inhomogeneities in the ionizing photon rate from particle to particle varies as a function of particle mass by carrying out another idealized Monte Carlo experiment. We again divide a stellar mass budget of  $10^7 M_\odot$  into particles of mass  $m_{\text{part}}$ . We populate these with stellar masses drawn from the IMF using the adjusted target scheme. We can then obtain the ionizing photon rate,  $S_{*,\text{part}}$ , for the particles at  $t_{\text{part}} = 0$  by summing the contributions from their component stars, as is done in the simulation. To enable comparison between different particle masses, we then obtain the specific ionizing photon rate,  $s_{*,\text{part}} = S_{*,\text{part}}/m_{\text{part}}$ , for each particle. Fig. 11 shows PDFs of  $s_{*,\text{part}}$  for the ensemble of particles at a given  $m_{\text{part}}$ , normalized by the IMF averaged specific ionizing photon rate,  $s_{*,\text{IMFav}}$ . Therefore, the spread around unity indicates the level of inhomogeneities amongst the population of star particles compared to using the same IMF averaged ionizing photon rate for all particles. It is possible for a star particle to have an ionizing luminosity of zero because it has not been assigned any stars more massive than  $7 M_\odot$ . Below this mass we assume the star emits no ionizing photons for simplicity. The ionizing luminosity is already negligible at this mass so this is not an issue, but this does result in a discrete feature at  $s_{*,\text{part}} = 0$  which cannot be meaningfully represented in our logarithmic PDFs. We therefore include an inset figure that shows the probability that a particle has an ionizing luminosity of zero. Thus the integral under the PDF and the value of corresponding bar in the inset plot sum to unity together.

As expected, Fig. 11 shows that the spread around the IMF averaged specific luminosity reduces as the particle mass increases. This is because the IMF is more completely sampled within the particle for a larger particle mass i.e.  $s_{*,\text{part}}$  converges with  $s_{*,\text{IMFav}}$  as  $m_{\text{part}}$  goes to infinity. It is important to note that this does not mean that inhomogeneities are not important, rather that a simulation with a large particle mass is incapable of resolving them. If the particle mass is large enough that inhomogeneities vanish, then using IMF averaged values will not result in any further loss of fidelity in the simulation and so this simpler approach can be adopted. With  $m_{\text{part}} = 10^4 M_\odot$ , the largest particle mass we consider, each particle samples the IMF relatively well, so  $s_{*,\text{part}}$  is very tightly distributed about the IMF average, deviating by a factor of 2 at most. However, as the particle mass decreases, the spread about the IMF averaged value is no longer insignificant. It already begins to span a factor of a few when  $m_{\text{part}} = 10^3 M_\odot$ . The distribution continues to become broader and flatter as the particle mass as further decreased. A sharp cutoff is apparent at the low end of the PDF. As mentioned before, this originates from particles that are assigned no ionizing sources. The smallest non-zero  $s_{*,\text{part}}$  corresponds to the emission from a single  $7 M_\odot$  in the particle, so this cutoff occurs at higher values of  $s_{*,\text{part}}$  for lower  $m_{\text{part}}$ . Correspondingly, the fraction of particles that produce no ionizing radiation (the inset panel) increases with decreasing  $m_{\text{part}}$ , such that when  $m_{\text{part}} = 20 M_\odot$  only approximately a quarter of particles produce radiation. However, even if particles do emit radiation, when  $s_{*,\text{part}}$  is more than factor of a few below the IMF averaged value this emission is negligible.

The top end of the PDFs represent the rare bright sources. It can be seen that with  $m_{\text{part}} = 300 M_{\odot}$ , some particles can have a specific ionizing luminosity an order of magnitude larger than the IMF averaged value. The maximum physically obtainable specific ionizing luminosity for the stellar mass range we consider corresponds to emission from a  $100 M_{\odot}$  star. This is 18.47 times the IMF averaged value.<sup>7</sup> This limit is indicated with a dashed line in Fig. 11. Low mass particles can exceed this limit when they are assigned more stellar mass than their dynamical mass (a natural consequence of our IMF sampling scheme which is not particularly problematic, as discussed in Section 2). Note that this does not result in an unphysically bright source in the simulation or affect the clustering of bright sources. It simply indicates that a more physically correct determination of their specific ionizing luminosity should account for the particles that have a mass discrepancy in the opposite sense, created by the adjusted target IMF sampling scheme to ensure mass consistency over multiple particles.

Fig. 11 demonstrates quantitatively how the ability to resolve inhomogeneities in the strength of ionizing sources varies as a function of particle mass. Similar scalings will result from any feedback source and are relatively easy to determine. However, the impact of the inhomogeneities on the outcome of the simulation are harder to predict. By averaging over the IMF, one gains more sources that have the IMF averaged feedback strength at the cost of losing the strongest sources. In our simulations, using IMF averaged ionizing photon rates results in more efficient feedback. This is because a source with the IMF averaged rate is still able to start forming a resolvable H II region and such sources are typically present earlier in the life of a star forming cloud, so the penalty incurred by losing the brightest sources is outweighed by benefits of increasing the overall number of ionizing sources. This positive impact on the overall feedback strength of IMF averaging will not necessarily occur in all scenarios. If the IMF averaged ionizing photon rate was not enough to form a resolvable H II region (e.g. because of a different resolution, star formation prescription etc.) then the reverse could occur since the simulation would contain no sources bright enough to have an impact. Note also that in simulations of an individual GMC at a *higher* resolution than us, Grudić & Hopkins (2019) found the opposite trend (i.e. more discretization of ionizing sources leads to more effective feedback). Thus, it is difficult to predict the impact of IMF averaging vs. sampling in a given simulation. However, we would suggest that as the latter is arguably more physical it should in general be adopted if there will be significant particle to particle inhomogeneities.

These arguments apply to all forms of non-SN stellar feedback, not just ionizing radiation. We possibly see the reverse trend affecting our photoelectric heating feedback in our simulations than affects photoionization feedback. Photoelectric heating is very ineffective in our simulations of dwarf galaxies, as can be seen in Fig 5. This is because of the low dust-to-gas ratio (as discussed in Paper I). The sim-

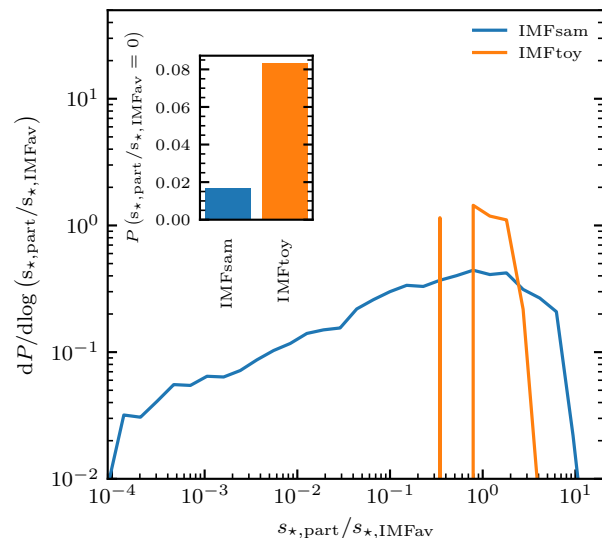


**Figure 12.** Similar to Fig. 11, the distribution of the specific ionizing luminosity, normalized by the IMF average, for a  $10^7 M_{\odot}$  population of star particles. In this plot we show the results for  $250 M_{\odot}$  particles with their luminosity obtained by explicitly populating the particles from the IMF (*IMFsam*) or by using the toy model of Su et al. (2018) to modulate the IMF averaged rates (*IMFtoy*). The toy model results in a much narrower distribution than that which arises from sampling the IMF directly because it does not account for the substantial variation in the luminosity of massive stars as a function of mass. Note that the toy model forces the particles to adopt one of a discrete set of luminosities, so plotting this as a PDF is sub-optimal but we do so to enable easy comparison to Fig. 11.

ulations with photoelectric heating alone have similar SFRs to the simulation without any feedback. Nonetheless, the peak SFR in the *IMFsam* version is marginally lower than the *IMFav* equivalent, possibly indicating that IMF averaging weakens the photoelectric heating feedback, in contrast to the photoionization feedback which is strengthened. This could occur if only the brightest sources were able to cause sufficient heating to have an impact and that spreading their luminosity among multiple sources (via IMF averaging) renders heating ineffective. However, we caution that the difference is very slight and these galaxies are already in an unphysical regime, having fragmented into very dense clouds and reached a very high SFR due to ineffective feedback.

#### 4.2.2 Can a simplified model be used to replicate the effects of explicit IMF sampling?

Su et al. (2018) examines how discretizing stellar feedback affects dwarf galaxies, in this case with cosmological zoom-in simulations with a mass resolution of  $250 M_{\odot}$ . In common with the other works previously mentioned, they find that modelling SNe as a continuous injection of feedback, rather than as discrete events, substantially weakens its impact. Yet, in contrast to us, they find that the efficiency of continuous non-SN feedback mechanisms (e.g. radiation and stellar winds) are largely unaffected by accounting for the effects of IMF sampling as opposed to their default IMF averaged rates. This could indicate that the impact of the particle

<sup>7</sup> We confirmed in test simulations for Paper I that our results are relatively insensitive to dropping this maximum stellar mass to  $50 M_{\odot}$ , which corresponds to a specific ionizing luminosity relative to the IMF average of 9.65.

to particle inhomogeneities do not result in a resolvable effect at their mass resolution. However, they do not actually perform explicit IMF sampling but instead attempt to replicate the effects via a toy model. At the point of creation, a star particle is assigned a number of O stars,  $N_O$ , drawn from a Poisson distribution with an expectation value of  $\langle N_O \rangle = m_{\text{part}}/100 M_\odot$ . Their feedback schemes then operate as in the fiducial case, but all IMF averaged rates that are linked to massive stars (photoionization, photoelectric heating, UV radiation pressure, OB star winds and core-collapse SN rates) are multiplied by a factor  $N_O/\langle N_O \rangle$ . When a SN occurs,  $N_O$  is reduced by one. It can therefore be seen that the strength of feedback will vary from star particle to particle according to the number of assigned sub-grid O stars, but the net rates over multiple particles will maintain the IMF average. This scheme is much simpler than explicitly sampling, assigning individual stars to particles and looking up their individual feedback budgets. The downside is that the approximation does not completely capture the correct behaviour, for a number of reasons. As we have demonstrated in the previous section, stochastically triggering SNe from IMF averaged SN rates already captures the correct clustering properties, as would be produced by explicit IMF sampling.<sup>8</sup> Thus, boosting the IMF averaged SN rates will result in an additional over-enhancement of clustering.

A potentially more problematic issue with the approximation is that it assumes massive stars are uniform in terms of their feedback budget, as the authors caution. A large amount of the scatter in the specific ionizing luminosity of a star particle (shown in Fig. 11) originates not just from the variation in the number of massive stars assigned to a star particle but also from the strong mass dependence of the ionizing luminosity produced by individual stars. In other words, there is a significant variation in luminosity among OB stars. Fig. 12 shows the results of a similar Monte Carlo experiment, where we assign a  $t_{\text{part}} = 0$  ionizing photon rate to  $250 M_\odot$  star particles either by populating them with stars sampled from the IMF, as usual, or by using the toy model of Su et al. (2018). It can be seen that the toy model is not a good approximation to the correct distribution, with a much narrower range of ionizing photon rates, producing far more stars close to the IMF average value and lacking the brightest sources.

Additional inconsistencies in the toy model arise as the star particles age. The multiplicative factor that modulates the feedback rates is reduced by  $1/\langle N_O \rangle$  when a SN occurs, regardless of when it occurs. An early SN indicates a more massive progenitor, which in turn means a larger drop in the ionizing photon budget for the particle. This decrease in luminosity as the most massive stars die is already accounted for in the time evolution of the IMF averaged rates. Another direct consequence of the link between lifetime, stellar mass and photon budget is that the earliest SNe should occur in regions that have been exposed to the highest ionizing flux, an effect not captured by the toy model. All of these

issues taken together, but in particular that shown in Fig. 12, suggest that IMF sampling effects likely cannot be replicated by simply modulating the IMF averaged rates.

## 5 SUMMARY AND CONCLUSIONS

It is a common practice in simulations of galaxies to treat stellar mass in a homogenised manner, with star particles producing IMF averaged feedback. With the advent of simulations with increasingly higher baryonic mass resolution, we have examined the extent to which this approximation is valid and under what circumstances it breaks down. We began by exploring methods of populating star particles with inventories of stars drawn from the IMF. Because of the challenges of filling an arbitrary mass budget with a discrete set of randomly drawn stellar masses, the goals of conserving mass (globally and locally) and faithfully reproducing the input IMF are often in tension. We argued that because the IMF is almost never an emergent property because of resolution limits and missing physics, an input IMF must be provided and reproduced accurately by the sampling scheme. This IMF may be fixed or it can vary based on some sub-grid prescription, but it should not be biased by numerical issues such as the choice of star particle mass, since this will affect the feedback budget. Sampling schemes must therefore prioritise reproduction of the IMF and the conservation of mass across a population of star particles over ensuring that the mass of the stellar inventory assigned to the particle is consistent with the dynamical mass of the particle. Because exact N-body dynamics of individual stars are generally unresolved in galaxy formation simulations, such a mass discrepancy is in general unimportant as long as an effort is made to minimize it. The discrepancy can also be resolved by allowing additional mass transfer to/between star particles, but this brings its own complexities and issues. Instead, we consider simple schemes that can easily be incorporated into existing star formation implementations without mass transfer. We carry out a series of Monte Carlo experiments to demonstrate the properties of these schemes, with the following results:

- Schemes that populate each star particle in isolation (i.e. without taking into account how other particles were populated) inevitably bias the IMF. The stop before approach, which throws away the last drawn stellar mass (that which carries the total assigned mass over the target), over-produces low mass stars and suppresses the high mass end of the IMF. The stop after approach, which always keeps the last draw, reproduces the shape of the IMF but results in too high a normalization, over-producing stars of all masses. The stop nearest approach, which retains a draw if keeping it results in a total assigned mass that is closer to the target, suffers from the same biases as the stop before scheme, albeit to a lesser extent.

- Because they fail to accurately reproduce the IMF, all of these schemes result in an incorrect feedback budget. The relative size of this error diminishes with increasing particle mass, but is still apparent when the particles have a mass of a few hundreds of  $M_\odot$ .

- We propose a scheme, which we refer to as adjusted target, that takes into account the degree to which previous particles overshot their target and selects a new target mass to compensate. Thus some star particles have more stellar

<sup>8</sup> As we have already discussed at length, this is true only if the sampling is carried out consistently. Su et al. (2018) use Bernoulli trials. The combination of their particle mass and typical time-step yields  $\bar{N}_{\text{SN}} \sim 10^{-5}$ , which is sufficiently small for Bernoulli trials and Poisson sampling to converge.

mass assigned than their dynamical mass while the reverse is true for others, but the mass discrepancy is always minimized as much as possible. Our scheme results in the input IMF being perfectly reproduced for all star particle masses and produces the correct feedback budget (e.g. the number and timing of SNe, the amount of ionizing radiation etc.).

In the second part of this work, we carried out isolated simulations of an  $M_{\text{vir}} = 10^{10} M_{\odot}$  dwarf galaxy with a baryonic mass resolution of  $20 M_{\odot}$ . We included stellar feedback in the form of core-collapse SNe, photoionizing radiation and photoelectric heating, treated with the new sub-grid models described in [Paper I](#) and implemented in the AREPO code. We compared two sets of simulations that either used IMF averaged rates for feedback or explicitly populated particles with discrete stars (using the adjusted target method). Our key findings are as follows:

- If SNe are the only source of stellar feedback, triggering individual SNe via Poisson sampling of IMF averaged rates yields identical results to explicitly sampling stellar masses from the IMF. This is because the distribution of the SNe in space and time is essentially perfectly reproduced by a stochastic sampling of the rates as long as the time resolution is sufficiently high.
- The impact of ionizing radiation is overestimated in our simulations when IMF averaged rates are adopted, particularly its ability to regulate SFRs. Approximately twice the mass of gas is photoionized per unit stellar mass when the IMF averaged rates are used compared to the explicit IMF sampling equivalent simulations. This is because the latter scheme correctly produces brighter but, crucially, rarer sources. For our adopted resolution, the IMF averaged ionizing photon rate emitted from a star particle within the first few Myrs after its creation is sufficient to photoionize a gas cell, as long as the gas has not collapsed significantly beyond the onset of star formation. This density condition is almost always fulfilled, because every star particle is an ionizing source meaning that clumps of gas begin to have their collapse disrupted as soon as star formation begins. This results in the production of many small H II regions. By contrast, IMF sampling means that only star particles that contain the relatively rare, bright sources are able to start photoionizing gas, meaning that not every star particle can disrupt a cloud. This results in less efficient feedback and fewer but larger H II regions.
- The scenario we see in these simulations is not necessarily ubiquitous. The degree to which the strength of IMF averaged feedback deviates from the explicitly sampled case depends on a number of factors. Firstly, the star particle must be of a sufficiently small mass such that appreciable inhomogeneities are apparent across the population of star particles. This will vary between different feedback channels. Secondly, the impact of these inhomogeneities must itself be resolvable in the simulation. IMF averaging may also potentially decrease the effectiveness of feedback under certain conditions. Feedback strength goes up in our simulations when we use IMF averaging because the resultant ionizing luminosity remains high enough to have an impact. We thus increase the number of effective sources of feedback, despite the penalty of losing the strongest sources. However, if a feedback channel is completely dependent on extremely rare, strong sources (e.g. the most massive O stars), then

IMF averaging may result in a net reduction in the feedback strength.

Given the complex dependence on resolution, the details of sub-grid models and the highly non-linear behaviour of stellar feedback, it is difficult to predict a priori whether there will be a difference between an IMF averaged feedback scheme and an IMF sampled scheme in any given simulation. However, the IMF sampling approach is always the more physically motivated approach. In other words, the best an IMF averaged scheme can achieve is to give results that converge with an IMF sampling approach. Even then, it will only converge when the effects of sampling are unresolvable and thus no more fidelity can be gained by explicitly populating star particles with discrete stars. Therefore, rather than trying to estimate how much of an effect choosing IMF averaging over sampling will have on the resolved feedback a priori, we suggest that the choice should simply be based on the level of inhomogeneities between particles for the chosen particle mass. This varies between different feedback channels, but based on the variation in the specific ionizing luminosity between particles (see [Fig. 11](#)), we very conservatively suggest that explicit IMF sampling should be used when the particle mass is less than  $\sim 500 M_{\odot}$ .

In this work, we have used a single, fixed IMF ([Kroupa 2001](#)) in our tests. However, as we discussed, our techniques and findings are applicable to any IMF, including those that can vary based on local properties. Variable IMFs can already be adopted by IMF averaged feedback schemes by adding additional dimensions to lookup tables, but they can be treated in a very natural fashion by explicit sampling schemes, allowing very fine grained control of stellar populations on-the-fly. This would be an interesting avenue of future research. We have also only considered single stars. The sampling scheme could be extended to explicitly account for binary systems. The inclusion of binary stellar evolution results in a modest increase in the total ionizing photon budget and extends the production of ionizing radiation to later times (see e.g. [Eldridge & Stanway 2009](#)), as well as introducing an additional population of late-time core-collapse SNe ([Zapartas et al. 2017](#)). It would also allow feedback channels that depend on binary systems (e.g. Type Ia SNe, jets from High Mass X-ray Binaries and OB runaways etc.) to be treated in a self-consistent manner. Thus, using explicit IMF sampling in galaxy formation simulations not only allows us to capture the inhomogeneous distribution of stellar feedback sources but may also provide a more direct link to models of stellar evolution than IMF averaged approaches.

## ACKNOWLEDGEMENTS

The author is grateful to Elaad Applebaum, John Forbes and Chia-Yu Hu for helpful discussions and to Rachel Somerville and Greg Bryan for comments which improved this manuscript. The work of M.C.S. was supported by a grant from the Simons Foundation (CCA 668771, L.E.H.). The simulations were run on the Flatiron Institute’s research computing facilities (Iron and Popeye compute clusters), supported by the Simons Foundation.

## DATA AVAILABILITY STATEMENT

The data underlying this article will be shared on reasonable request to the corresponding author.



## REFERENCES

- Agertz O., Kravtsov A. V., 2015, *ApJ*, **804**, 18
- Andrews J. E., et al., 2013, *ApJ*, **767**, 51
- Andrews J. E., et al., 2014, *ApJ*, **793**, 4
- Applebaum E., Brooks A. M., Quinn T. R., Christensen C. R., 2020, *MNRAS*, **492**, 8
- Bressan A., Marigo P., Girardi L., Salasnich B., Dal Cero C., Rubele S., Nanni A., 2012, *MNRAS*, **427**, 127
- Calzetti D., Chandar R., Lee J. C., Elmegreen B. G., Kennicutt R. C., Whitmore B., 2010, *ApJ*, **719**, L158
- Cappellari M., et al., 2012, *Nature*, **484**, 485
- Carigi L., Hernandez X., 2008, *MNRAS*, **390**, 582
- Ceverino D., Klypin A., Klimek E. S., Trujillo-Gomez S., Churchill C. W., Primack J., Dekel A., 2014, *MNRAS*, **442**, 1545
- Chabrier G., 2003, *PASP*, **115**, 763
- Chieffi A., Limongi M., 2004, *ApJ*, **608**, 405
- Conroy C., van Dokkum P. G., 2012, *ApJ*, **760**, 71
- Corbelli E., Verley S., Elmegreen B. G., Giovanardi C., 2009, *A&A*, **495**, 479
- Davé R., Thompson R., Hopkins P. F., 2016, *MNRAS*, **462**, 3265
- Davé R., Anglés-Alcázar D., Narayanan D., Li Q., Rafieferantsoa M. H., Appleby S., 2019, *MNRAS*, **486**, 2827
- Dubois Y., et al., 2014, *MNRAS*, **444**, 1453
- Dubois Y., Peirani S., Pichon C., Devriendt J., Gavazzi R., Welker C., Volonteri M., 2016, *MNRAS*, **463**, 3948
- El-Badry K., Ostriker E. C., Kim C.-G., Quataert E., Weisz D. R., 2019, *MNRAS*, **490**, 1961
- Eldridge J. J., Stanway E. R., 2009, *MNRAS*, **400**, 1019
- Elmegreen B. G., 2006, *ApJ*, **648**, 572
- Emerick A., Bryan G. L., Mac Low M.-M., 2019, *MNRAS*, **482**, 1304
- Fielding D., Quataert E., Martizzi D., Faucher-Giguère C.-A., 2017, *MNRAS*, **470**, L39
- Fielding D., Quataert E., Martizzi D., 2018, *MNRAS*, **481**, 3325
- Fujimoto Y., Krumholz M. R., Tachibana S., 2018, *MNRAS*, **480**, 4025
- Fumagalli M., da Silva R. L., Krumholz M. R., 2011, *ApJ*, **741**, L26
- Gatto A., et al., 2017, *MNRAS*, **466**, 1903
- Geen S., Watson S. K., Rosdahl J., Bieri R., Klessen R. S., Hénnebelle P., 2018, *MNRAS*, **481**, 2548
- Geha M., et al., 2013, *ApJ*, **771**, 29
- Genel S., et al., 2019, *ApJ*, **871**, 21
- Gentry E. S., Krumholz M. R., Dekel A., Madau P., 2017, *MNRAS*, **465**, 2471
- Gentry E. S., Krumholz M. R., Madau P., Lupi A., 2019, *MNRAS*, **483**, 3647
- Grudić M. Y., Hopkins P. F., 2019, *MNRAS*, **488**, 2970
- Gunawardhana M. L. P., et al., 2011, *MNRAS*, **415**, 1647
- Gutcke T. A., Springel V., 2019, *MNRAS*, **482**, 118
- Gutcke T. A., Pakmor R., Naab T., Springel V., 2020, arXiv e-prints, p. [arXiv:2010.07311](https://arxiv.org/abs/2010.07311)
- Haardt F., Madau P., 2012, *ApJ*, **746**, 125
- Haas M. R., Anders P., 2010, *A&A*, **512**, A79
- Hernquist L., 1990, *ApJ*, **356**, 359
- Hirai Y., Fujii M. S., Saitoh T. R., 2020, arXiv e-prints, p. [arXiv:2005.12906](https://arxiv.org/abs/2005.12906)
- Hopkins P. F., Kereš D., Oñorbe J., Faucher-Giguère C.-A., Quataert E., Murray N., Bullock J. S., 2014, *MNRAS*, **445**, 581
- Hopkins P. F., et al., 2018, *MNRAS*, **480**, 800
- Hoversten E. A., Glazebrook K., 2008, *ApJ*, **675**, 163
- Hu C.-Y., 2019, *MNRAS*, **483**, 3363
- Hu C.-Y., Naab T., Glover S. C. O., Walch S., Clark P. C., 2017, *MNRAS*, **471**, 2151
- Kalirai J. S., et al., 2013, *ApJ*, **763**, 110
- Katz N., 1992, *ApJ*, **391**, 502
- Katz N., Weinberg D. H., Hernquist L., 1996, *ApJS*, **105**, 19
- Keller B. W., Kruijssen J. M. D., 2020, arXiv e-prints, p. [arXiv:2004.03608](https://arxiv.org/abs/2004.03608)
- Keller B. W., Wadsley J. W., Wang L., Kruijssen J. M. D., 2019, *MNRAS*, **482**, 2244
- Kimm T., Cen R., Devriendt J., Dubois Y., Slyz A., 2015, *MNRAS*, **451**, 2900
- Kroupa P., 2001, *MNRAS*, **322**, 231
- Kroupa P., Weidner C., 2003, *ApJ*, **598**, 1076
- Kroupa P., Tout C. A., Gilmore G., 1993, *MNRAS*, **262**, 545
- Krumholz M. R., Tan J. C., 2007, *ApJ*, **654**, 304
- La Barbera F., Ferreras I., Vazdekis A., de la Rosa I. G., de Carvalho R. R., Trevisan M., Falcón-Barroso J., Ricciardelli E., 2013, *MNRAS*, **433**, 3017
- Lanz T., Hubeny I., 2003, *ApJS*, **146**, 417
- Lee J. C., et al., 2009, *ApJ*, **706**, 599
- Lee J. C., Veilleux S., McDonald M., Hilbert B., 2016, *ApJ*, **817**, 177
- Mac Low M.-M., McCray R., 1988, *ApJ*, **324**, 776
- Marinacci F., Sales L. V., Vogelsberger M., Torrey P., Springel V., 2019, arXiv e-prints, p. [arXiv:1905.08806](https://arxiv.org/abs/1905.08806)
- Meurer G. R., et al., 2009, *ApJ*, **695**, 765
- Mihos J. C., Hernquist L., 1994, *ApJ*, **437**, 611
- Naab T., Ostriker J. P., 2017, *ARA&A*, **55**, 59
- Navarro J. F., White S. D. M., 1993, *MNRAS*, **265**, 271
- Navarro J., Frenk C. S., White S. D. M., 1997, *ApJ*, **490**, 493
- Pakmor R., Springel V., Bauer A., Mocz P., Muñoz D. J., Ohlmann S. T., Schaal K., Zhu C., 2016, *MNRAS*, **455**, 1134
- Pillepich A., et al., 2018, *MNRAS*, **473**, 4077
- Rahmati A., Pawlik A. H., Raičević M., Schaye J., 2013, *MNRAS*, **430**, 2427
- Rémy-Ruyer A., et al., 2014, *A&A*, **563**, A31
- Revaz Y., Arnaudon A., Nichols M., Bonvin V., Jablonka P., 2016, *A&A*, **588**, A21
- Salpeter E. E., 1955, *ApJ*, **121**, 161
- Sharma P., Roy A., Nath B. B., Shchekinov Y., 2014, *MNRAS*, **443**, 3463
- Smith B. D., et al., 2017, *MNRAS*, **466**, 2217
- Smith M. C., Sijacki D., Shen S., 2018, *MNRAS*, **478**, 302
- Smith M. C., Bryan G. L., Somerville R. S., Hu C.-Y., Teyssier R., Burkhardt B., Hernquist L., 2020, arXiv e-prints, p. [arXiv:2009.11309](https://arxiv.org/abs/2009.11309)
- Somerville R. S., Davé R., 2015, *ARA&A*, **53**, 51
- Sormani M. C., Treß R. G., Klessen R. S., Glover S. C. O., 2017, *MNRAS*, **466**, 407
- Springel V., 2010, *MNRAS*, **401**, 791
- Springel V., Hernquist L., 2003, *MNRAS*, **339**, 289
- Springel V., Di Matteo T., Hernquist L., 2005, *MNRAS*, **361**, 776
- Stinson G., Seth A., Katz N., Wadsley J., Governato F., Quinn T., 2006, *MNRAS*, **373**, 1074
- Stinson G. S., Bailin J., Couchman H., Wadsley J., Shen S., Nickerson S., Brook C., Quinn T., 2010, *MNRAS*, **408**, 812
- Su K.-Y., et al., 2018, *MNRAS*, **480**, 1666
- Vogelsberger M., Genel S., Sijacki D., Torrey P., Springel V., Hernquist L., 2013, *MNRAS*, **436**, 3031
- Vogelsberger M., et al., 2014, *MNRAS*, **444**, 1518
- Weidner C., Kroupa P., 2006, *MNRAS*, **365**, 1333
- Weidner C., Kroupa P., Bonnell I. A. D., 2010, *MNRAS*, **401**, 275
- Weidner C., Kroupa P., Pflamm-Altenburg J., 2013, *MNRAS*, **434**, 84
- Yadav N., Mukherjee D., Sharma P., Nath B. B., 2017, *MNRAS*, **465**, 1720
- Zapartas E., et al., 2017, *A&A*, **601**, A29
- van Dokkum P. G., Conroy C., 2010, *Nature*, **468**, 940

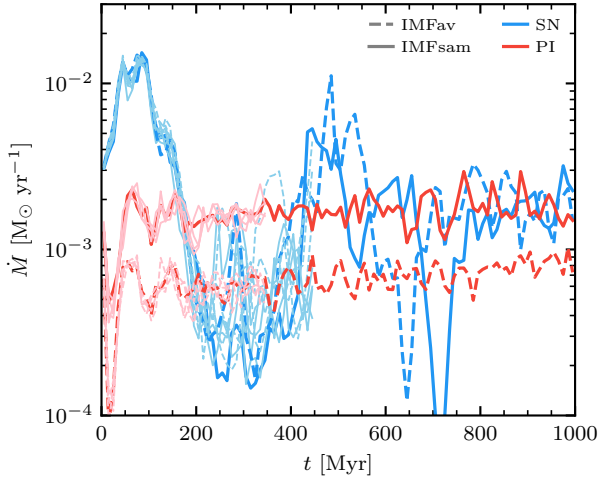


**Figure A1.** SFRs for our perturbed re-simulations (in the lighter shades) with the fiducial simulations for comparison (bold colours). The *IMFav* and *IMFsam* SN simulations are consistent with each other within the magnitude of the scatter between re-simulations. By contrast, the differences between the *IMFav* and *IMFsam* PI simulations are much larger than the scatter within a set of re-simulations.

## APPENDIX A: ROBUSTNESS TO STOCHASTICITY

Simulations of galaxy evolution are inherently chaotic to some degree, meaning that small perturbations introduced by, for example, seemingly minor differences in initial conditions, choice of random number generator seed value, floating-point round-off and non-deterministic behaviour of parallelised codes can lead to measurable large scale differences in the outcome (Keller et al. 2019; Genel et al. 2019). In order to approximately assess how the differences between our various feedback schemes compare to the magnitude of this stochastic uncertainty, we perform some re-simulations of the early stages of the *SN* and *PI* simulations with both the *IMFav* and *IMFsam* schemes. For each fiducial simulation, we carry out four additional re-simulations. In each re-simulation we use different seed values for random number generators. We also perturb the position of every gas cell, star particle and dark matter particle in the initial conditions by moving it 0.1 pc in a random direction. The SFRs for these simulations can be seen in Fig. A1, with the fiducial simulations shown in the bold colours and the re-simulations shown in a lighter shade.

We were limited by computational expense from completely re-simulating the full 1 Gyr of our fiducial simulations, but it can be seen that for the 450 Myr re-simulated the *IMFav* and *IMFsam* SN simulations are consistent with each other within the range of stochastic scatter. We are therefore confident in our assertion that IMF averaging and IMF sampling give essentially identical results if SNe are the only source of feedback. The *PI* re-simulations have a very tight scatter about the fiducial simulations, such that the magnitude of the stochastic uncertainty is much smaller than the difference between the *IMFav* and *IMFsam* schemes.